THE ASTROPHYSICAL JOURNAL, 458:761–782, 1996 February 20

GODDARD HIGH-RESOLUTION SPECTROGRAPH OBSERVATIONS OF PROCYON AND HR 1099[1]

BRIAN E. WOOD, GRAHAM M. HARPER, AND JEFFREY L. LINSKY[2]
JILA, University of Colorado, Boulder, CO 80309-0440; wood@marmot.colorado.edu, gmh@capybara.colorado.edu, jlinsky@jila.colorado.edu

AND

ROBERT C. DEMPSEY
Astronomy Programs, Computer Sciences Corporation, Space Telescope Science Institute, 3700 San Martin Drive, Baltimore, MD 21218; dempsey@stsci.edu
Received 1995 May 31; accepted 1995 August 29

ABSTRACT

Goddard High Resolution Spectrograph (GHRS) observations have revealed the presence of broad wings in the transition-region lines of AU Mic and Capella. It has been proposed that these wings are signatures of microflares in the transition regions of these stars and that the solar analog for this phenomenon might be the "transition region explosive events" discussed by Dere, Bartoe, & Brueckner. We have analyzed GHRS observations of Procyon (F5 IV–V) and HR 1099 (K1 IV + G5 IV) to search for broad wings in the UV emission lines of these stars. We find that the transition-region lines of HR 1099, which are emitted almost entirely by the K1 star, do indeed have broad wings that are even more prominent than those of AU Mic and Capella. This is consistent with the association of the broad wings with microflaring since HR 1099 is a very active binary system. In contrast, the transition-region lines of Procyon, a relatively inactive star, do not show evidence for broad wings, with the possible exception of N V λ1239. However, Procyon's lines do appear to have excess emission in their blue wings.

Linsky et al. found no evidence for broad wings in Capella's chromospheric lines, but we find that the Mg II resonance lines of HR 1099 do have broad wings. The striking resemblance between HR 1099's Mg II and C IV lines suggests that the Mg II line profiles may be regulated by turbulent processes similar to those that control the transition-region line profiles. If this is the case, microflaring may be occurring in the K1 star's chromosphere as well as in its transition region. However, radiative transfer calculations suggest that the broad wings of the Mg II lines can also result from normal chromospheric opacity effects rather than pure turbulence. The prominence of broad wings in the transition region and perhaps even chromospheric lines of active stars suggests that microflaring is very prevalent in the outer atmospheres of active stars.

Subject headings: line: formation — stars: chromospheres — stars: individual (α Canis Minoris, HR 1099) — ultraviolet: stars

1. INTRODUCTION

The Goddard High Resolution Spectrograph (GHRS) aboard the *Hubble Space Telescope* (*HST*) provides the sensitivity and spectral resolution necessary to study UV emission-line profiles that originate from stellar chromospheres and transition regions in much greater detail than heretofore possible. For example, using the GHRS, Linsky & Wood (1994) discovered that the C IV and Si IV lines of the very active dM0e star AU Mic are not Gaussian in shape but possess very broad wings. They hypothesized that the broad wings are signatures of microflares in the transition region of AU Mic and proposed that the solar analog for this phenomenon might be the "transition region explosive events" discussed by Dere, Bartoe, & Brueckner (1989). Linsky & Wood estimated the line flux originating from the microflares by fitting two Gaussians to the emission lines—a broad component representing the microflaring contribution and a narrow component representing the quiescent plasma's emission. The broad component accounted for ~40% of the C IV and Si IV line flux for AU Mic, whereas transition-region explosive events produce no more than 5% of the Sun's C IV and Si IV line flux (Dere et al. 1989). Compared to the Sun, the broad-component emission on AU Mic accounts for a far larger percentage of the transition-region line flux, which is reasonable because AU Mic is much more active than the Sun.

Broad wings have also been found in the transition-region lines of Capella (Linsky et al. 1995b). Because the G1 III star that dominates Capella's UV line emission is a very active star, Capella's transition-region line profiles were interpreted and modeled in the same manner as AU Mic's lines. The broad component's contribution to the line flux is correlated with line formation temperature, with this contribution ranging from 52% for N V λ1239 (log T = 5.25) to 24% for Si III λ1207 (log T = 4.7). No broad wings were detected in chromospheric lines such as the O I λ1300 triplet (log T ~ 4.0). Linsky et al. also noted that separating the G1 star's emission into broad and narrow components (and subtracting the emission from Capella's G8 III star) results in a smoother emission-measure distribution for the narrow component of the G1 star. The

[1] Based on observations with the NASA/ESA *Hubble Space Telescope*, obtained at the Space Telescope Science Institute, which is operated by the Association of Universities for Research in Astronomy, Inc., under NASA contract NAS5-26555.

[2] Staff member, Quantum Physics Division, National Institute of Standards and Technology, Boulder, CO 80309-0440.

emission-measure distribution of the broad component was found to resemble that of a sunspot.

In this paper we present and analyze GHRS observations of Procyon and HR 1099. One of our goals is to search for broad components in the UV emission lines of these stars. The hypothesis that the broad components are associated with microflaring suggests that the broad line wings are a manifestation of stellar activity and are prominent in the spectra of AU Mic and Capella because these are active stars. We would not expect to see broad wings in Procyon's transition-region lines that are as prominent as those seen for AU Mic and Capella because Procyon is significantly less active than these stars and is only a little more active than the Sun (Ayres, Marstad, & Linsky 1981). Therefore, our Procyon data will test the hypothesis that broad transition-region line wings are caused by microflaring.

Procyon (= α CMi = HD 61421) is a nearby (d = 3.5 pc) F5 IV–V star with a mass of 1.75 $M_\odot$ and a radius of 2.1 $R_\odot$ (Strand 1951; Steffen 1985; Irwin et al. 1992). The photospheric properties of Procyon have been exhaustively studied (e.g., Griffin 1971; Steffen 1985; Nordlund & Dravins 1990; Dravins & Nordlund 1990a, b), and Brown & Jordan (1981) have used *IUE* data to construct models of Procyon's chromosphere and transition region. An extensive, 24 day *IUE* observing campaign failed to detect any significant UV line flux variations, which suggests that the regions responsible for Procyon's UV emission lines uniformly cover the stellar surface (Ayres 1991). The coronal emission from Procyon has been measured by many X-ray and EUV instruments, including those aboard *Einstein*, *EXOSAT*, *ROSAT*, and the *Extreme-Ultraviolet Explorer* (*EUVE*) (Lemen et al. 1989; Wood et al. 1994; Drake, Laming, & Widing 1995).

HR 1099 (= V711 Tau = HD 22468) is an RS CVn binary system whose components have spectral types K1 IV and G5 IV, masses of 1.4 and 1.1 $M_\odot$, and radii of 3.9 and 1.3 $R_\odot$, respectively. This star system, which is located 36 pc away, has an orbital period of 2.84 days (Fekel 1983; Strassmeier et al. 1988). Optical spectroscopy and Doppler imaging techniques have revealed the presence of dark spots on the surface of the K1 star, which have been found to evolve with time (Bartolini et al. 1983). Ayres & Linsky (1982) found that the K1 star is responsible for most of HR 1099's UV emission-line flux. Further *IUE* observations have revealed variability in those lines on timescales ranging from days to years (Dorren & Guinan 1990). Analysis of HR 1099's extremely strong X-ray emission has revealed the presence of coronal temperatures at least as high as log T = 7.3 (Schmitt et al. 1990; Dempsey et al. 1993; Brown 1994).

Because of their rapid rotation, induced by tidal locking, RS CVn systems as a group are extremely active in terms of bright UV emission lines and variability, including flaring. HR 1099 is one of the most active of the RS CVn binaries and therefore represents an extreme of stellar activity. If stellar activity does indeed produce "broad components" in transition-region lines, one would anticipate that the broad components of HR 1099's lines should be at least as prominent as those found for AU Mic and Capella. Like Procyon, HR 1099 will therefore provide a test of the activity–broad component correlation. The desire to contrast the line profiles of a relatively inactive star with those of a very active star is the primary motivation for discussing the Procyon and HR 1099 observations in the same paper. In addition to the search for broad line wings, we will also discuss other interesting aspects of these data, including line redshifts and density diagnostics.

2. GHRS OBSERVATIONS OF PROCYON AND HR 1099

The GHRS observations of Procyon and HR 1099 are summarized in Table 1. (See Brandt et al. 1994 and Heap et al. 1995 for a description of the GHRS instrument and its capabilities prior to the installation of COSTAR.) In addition to the data listed in Table 1, several other GHRS observations of HR 1099 were made during the week of 1993 September 14–21, which provide more orbital phase coverage and provide the data necessary to investigate line variability. These additional data are discussed in detail by Dempsey, Neff, & Linsky (1996). All the observations of Procyon and HR 1099 were made prior to the 1993 December installation of COSTAR into *HST*, which significantly improved the spectral resolution of GHRS, especially for observations made through the large science aperture (LSA). The approximate spectral resolution of each of our pre-COSTAR observations is listed in Table 1.

Images of the platinum spectral-calibration lamp were taken in the wavelength regions of interest prior to most of our spectra to maximize the accuracy of our wavelength calibrations. The exceptions are the HR 1099 observations of the 1637–1672 and 1532–1568 Å spectral regions. For these spectra, the standard wavelength calibrations were used, but with offset corrections based on a wavelength-calibration image made before the source spectra with the same grating but of a different spectral region—a "spectrum y-balance," or SPYBAL, calibration image. (SPYBAL calibration spectra are used to properly center spectra on the diode array and are usually made whenever the observed wavelength region is changed.) The dispersion relations of the SPYBAL-calibrated spectra are roughly 3–10 times less accurate than those of the fully calibrated spectra, for which the dispersion relations should be accurate to much better than 1 km s^{-1} (Robinson et al. 1992). However, other sources of uncertainty, such as asymmetries in the aberrated point-spread function (Gilliland & Hulbert 1993) and possible inaccuracies in target centering, may produce larger errors than the uncertainties associated with the dispersion relations. For our moderate-resolution spectra, we estimate the accuracy of our wavelength calibrations to be ± 3 and ± 5 km s^{-1} for the fully calibrated and SPYBAL-calibrated spectra, respectively. The wavelength calibration of the echelle spectra should be good to within ± 1.5 km s^{-1} (Linsky et al. 1993).

Most of the spectra were taken in a series of at least two data readouts. Breaking up the observations in this fashion permitted us to check the individual readouts for systematic line shifts due to changes in the Earth's magnetic field and/or instrumental thermal drifts. We also could search for flux variations in the emission lines, which is especially useful for HR 1099, which flares frequently. However, no substantial line shifts or line flux variations were evident during any of the observations listed in Table 1. The G160M spectra of the 1205–1243 Å region for Procyon and HR 1099 were obtained using the FP-SPLIT mode, in which each observation consists of numerous readouts with the spectrum shifted on the diode array between readouts several times during the observation. This is the most accurate way to compensate for sensitivity variations among the detector diodes.

All of the observations in Table 1 are quarter-stepped spectra, meaning that each readout of each spectrum consists of four separate exposures on the GHRS detector's array of 500 science diodes, and the spectrum has been shifted between each exposure by one-quarter diode. Thus, the spectra were oversampled by a factor of 4, and the final spectra are arrays

TABLE 1

SUMMARY OF GHRS OBSERVATIONS

Grating	Aperture	Spectral Range (Å)	Spectral Resolution (km s^{-1})	Date	Orbital Phase	Exposure Time (s)	Start Time (UT)	Important Spectral Features
				Procyon				
G200M.....	LSA	1880–1920	20	1992 Dec 21	...	135	14:58	Si III], C III]
G160M.....	LSA	1623–1658	20	1992 Dec 21	...	592	15:56	He II
G160M.....	LSA	1532–1568	20	1992 Dec 21	...	377	16:09	C IV
G160M.....	LSA	1384–1420	20	1992 Dec 21	...	431	16:20	Si IV, O IV]
G160M.....	SSA	1205–1243	15	1992 Dec 21	...	3231	17:31	Si III, H I, O V], N V
EB-20	SSA	2792–2807	3.5	1992 Dec 21	...	646	19:27	Mg II
EB-22	SSA	2593–2605	3.3	1992 Dec 21	...	646	19:47	Fe II
				HR 1099				
G160M.....	SSA	1205–1243	15	1993 Sep 14	0.24	3916	18:51	Si III, H I, O V], N V
G200M.....	LSA	1880–1920	20	1993 Sep 18	1.64	489	19:19	Si III], C III]
G160M.....	LSA	1637–1672	20	1993 Sep 18	1.65	707	19:32	He II, C I, O III]
G160M.....	LSA	1532–1568	20	1993 Sep 18	1.66	816	20:36	C IV
G160M.....	LSA	1384–1420	20	1993 Sep 18	1.67	1197	20:53	Si IV, O IV]
EB-22	SSA	2593–2605	3.3	1993 Sep 19	1.73	979	1:18	Fe II
EB-20	SSA	2792–2807	3.5	1993 Sep 21	2.73	1414	21:05	Mg II

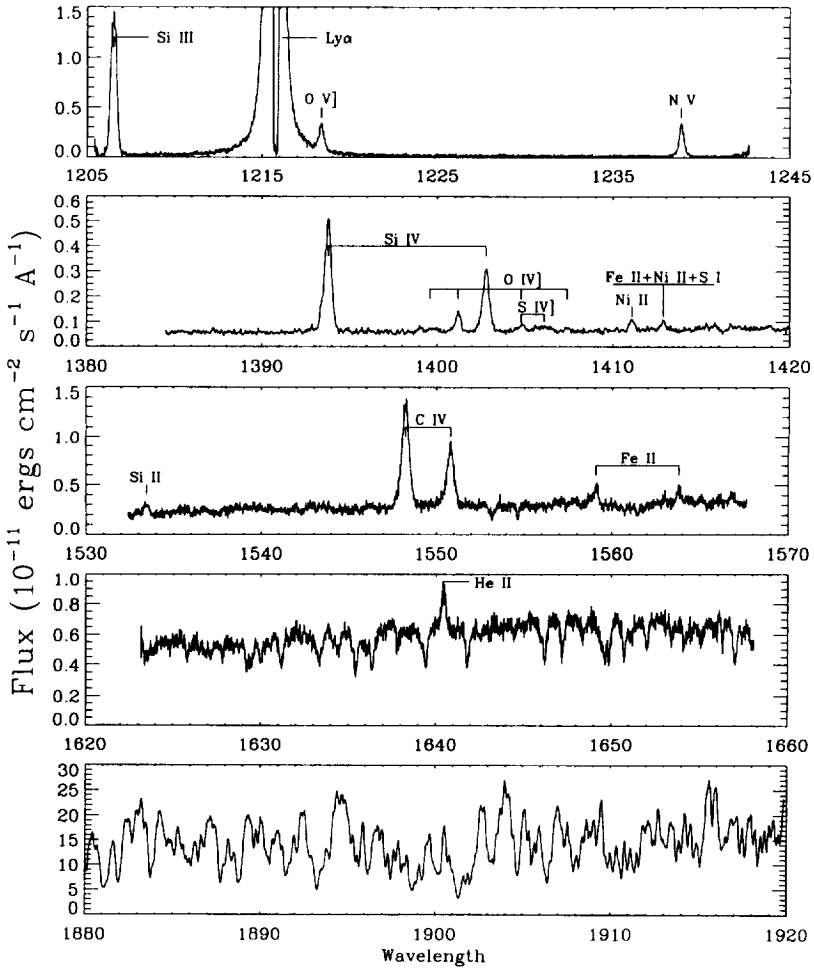

FIG. 1.—Moderate-resolution spectra of Procyon with line identifications. The 1384–1420 Å spectrum has been smoothed slightly to reveal the weak O IV] lines.

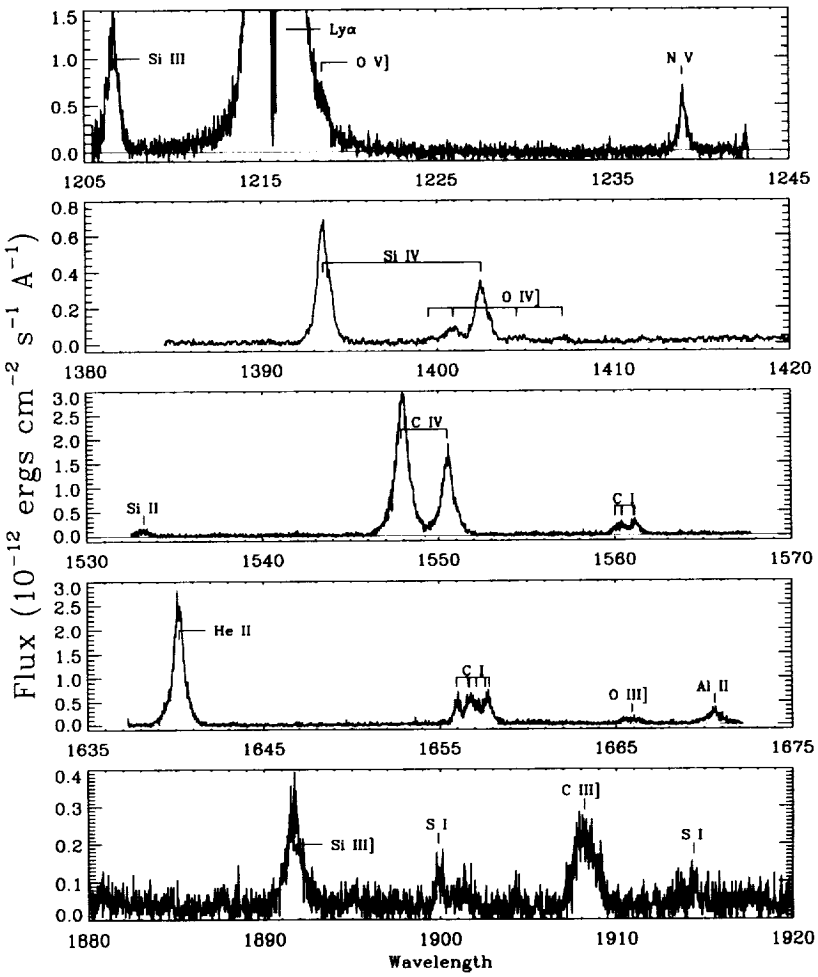

FIG. 2.—As Fig. 1, but for HR 1099

with 2000 elements. (The final FP-SPLIT spectra actually have more than 2000 elements because of the shifting of the spectrum on the diode array between readouts.)

The Procyon and HR 1099 data were processed with the 1993 September and 1993 December versions of the CALHRS calibration software, respectively (Duncan 1992). The sensitivities of the GHRS gratings are probably not known to better than $\pm 10\%$, so we estimate this to be the uncertainty in our flux calibrations. The moderate-resolution spectra are displayed in Figures 1 and 2. All obvious emission lines have been identified. The strong lines were previously identified and measured in *IUE* spectra (Brown & Jordan 1981; Simon & Linsky 1980). We used the solar spectrum (Sandlin et al. 1986) to help identify some of the weak lines. The echelle observations of the Mg II *h* and *k* lines of Procyon and HR 1099 are displayed in Figure 3. For Procyon, the interstellar absorption features found in Lyα, Mg II, and Fe II have already been analyzed by Linsky et al. (1995a). An analysis of similar features seen in the spectra of HR 1099 will be presented in a future paper.

3. ANALYSIS OF PROCYON DATA

3.1. *Line Profile Parameters and the Search for Broad Components*

The simplest way to characterize a symmetric line profile quantitatively is to measure the velocity, flux, and FWHM of the line, and one way to estimate these quantities is to fit a Gaussian to the line. We have fit single Gaussians to all of Procyon's emission lines using χ^2 minimization to determine the best fits (Bevington & Robinson 1992). The results of this procedure are summarized in Table 2. In the fitting process, each proposed fit was convolved with the instrumental profile extracted from Gilliland & Hulbert (1993) before testing the fit, in order to correct for instrumental broadening. The rest wavelengths assumed in this paper are the same as those used by Linsky et al. (1995b). The velocities listed in Table 2 assume a radial velocity for Procyon of -3.5 km s^{-1}, which was computed from the orbital parameters given by Irwin et al. (1992). The 1 σ random errors in the tabulated parameters have been computed following the prescription of Lenz & Ayres (1992), and the quality of the Gaussian fits is measured by the reduced χ^2 statistic listed in the last column of the table. A Gaussian fit was not performed for the Lyα line because of its non-Gaussian shape and strong interstellar absorption. We have estimated a flux for this line, however, using the correction for interstellar absorption adopted by Linsky et al. (1995a), which suggests that 47% of the stellar emission is absorbed by interstellar hydrogen. Inspection of the line wings has also provided an estimate of the line velocity (see Table 2). A similar procedure was used to estimate the velocities and fluxes of the Mg II *h* and *k* lines (see § 3.5). The fact that the Mg II and Lyα lines are well centered in the stellar rest frame suggests that our wavelength

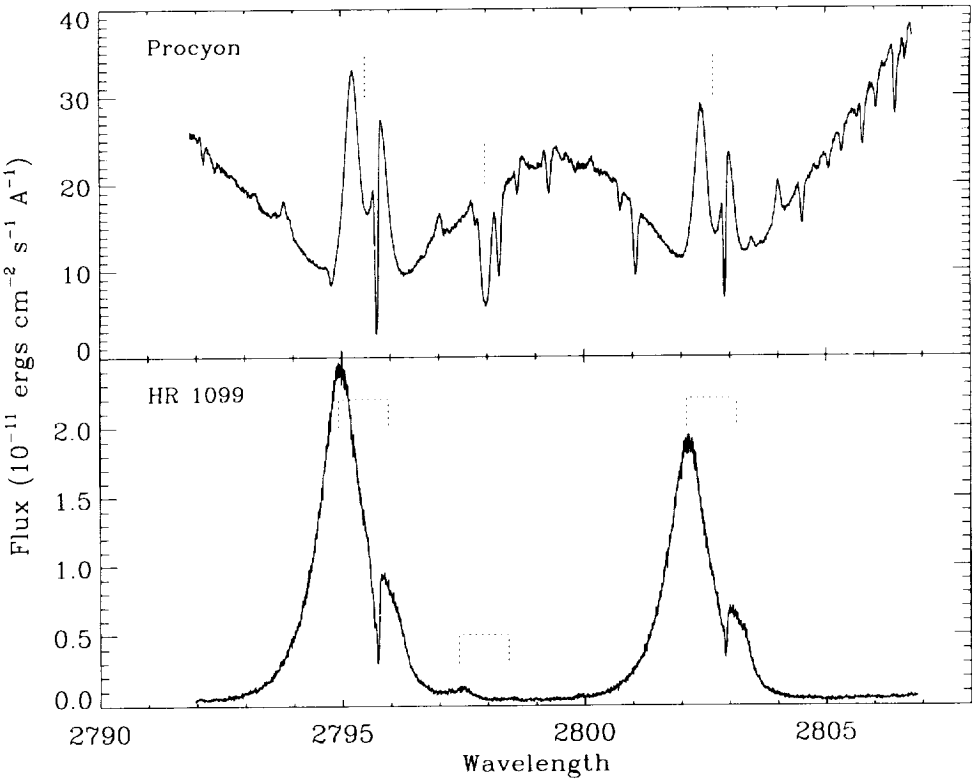

FIG. 3.—Echelle spectra of the Mg II *h* and *k* lines of Procyon (*top*) and HR 1099 (*bottom*). The dotted lines mark the rest wavelengths of the Mg II lines in the stellar rest frames. The line locations are marked for both stars of the HR 1099 system. Because of the orbital velocities of the two stars, the G5 star's lines are redshifted relative to the K1 star's lines. Besides the Mg II *h* and *k* lines at rest wavelengths of 2802.705 and 2795.528 Å, the location of the Mg II subordinate line at 2797.998 Å is indicated.

calibrations are very accurate.

Inspection of the profiles of the O V], N V, Si IV, and C IV lines revealed a blue-wing excess (see § 3.2), so the blue wing was not considered in the single-Gaussian fits to these lines. Figure 4 shows that when the blue wings are ignored, these lines are well fit by single Gaussians, with the exception of N V λ1239. According to the χ_ν^2 values in Table 2, all of the single-Gaussian fits to Procyon's emission lines are acceptable within the 2 σ criterion except for the fits to the Si III λ1207 and N V λ1239 lines. The non-Gaussian nature of the Si III line is probably due to appreciable opacity (see § 3.4). The non-Gaussian nature of the N V line is different, however, as it is the only line that seems to have excess flux in *both* wings. Opacity broadening cannot account for these broad wings for reasonably low optical depths, and N V should in any case be less optically thick than the Si III, Si IV, and C IV lines. We therefore interpret the broad wing emission as being indicative of a turbulent component to the N V line, and we fitted the N V line with two Gaussians. The results are illustrated in Figure 4*b* and Table 2. Monte Carlo simulations were used to estimate errors for the two-Gaussian fit parameters of N V. Because of the lack of excess emission in *both* wings of the Si IV and C IV lines and because these line profiles appear to be Gaussian everywhere except in the blue wings, we conclude that these lines do not have detectable "broad components" like those found in the lines of AU Mic and Capella. This is consistent with the association of the broad components with microflaring since Procyon is much less active than AU Mic and Capella.

The only emission line that seems to have a broad component is the N V λ1239 line, which is the highest temperature resonance line that we have observed, with a line formation temperature of log $T = 5.25$. This discovery is consistent with that of Linsky et al. (1995b), who found that the broad components of Capella's emission lines are strongest in the higher temperature lines. The O V] λ1218 line, which is formed at a temperature of about log $T = 5.4$, does not appear to have a broad component, but this is a low optical depth intersystem line rather than a resonance line like N V. If the microflares that are presumably responsible for the N V line's broad wing emission have high densities, collisional de-excitation could conceivably cause the flux emitted in the O V] line to be much less than that observed in N V. Since the O V] line is superposed upon the red wing of Lyα, we cannot assume a flat background as we have for the other lines but must instead use a polynomial fit to estimate the "continuum" for the line (see Fig. 4*a*). Because of the uneven continuum, this background estimation is more uncertain than for the other lines, meaning it is conceivable that the O V] line does in fact have a weak, undetected broad component. Linsky et al. (1995b) were unable to find evidence for broad wings in Capella's intersystem lines, but various difficulties prevented them from concluding that their data were inconsistent with the existence of broad components in those lines.

3.2. *Line Shifts and Blue-Wing Excesses*

Figure 5 illustrates the blue-wing excesses of the O V], N V, Si IV, and C IV lines by displaying the smoothed residuals of the fits shown in Figure 4. The velocity of the excess emission is about -90 km s^{-1}, and the emission is most apparent in the C IV lines and the stronger Si IV line. The Si III λ1207 line does

TABLE 2

LINE PROFILE PARAMETERS FOR PROCYON

Ion	log T[a]	λ_{rest} (Å)	λ_{meas} (Å)	v[b] (km s^{-1})	f (10^{-13})	FWHM (km s^{-1})	χ^2_ν
Single-Gaussian Fits							
Si III[c]	4.7	1206.510	1206.512	4 ± 1	57.7 ± 0.5	81 ± 2	1.492
H I[d]	4.2	1215.670	1215.658	0 ± 1	1300 ± 100	...	...
O V]	5.4	1218.344	1218.373	11 ± 1	8.4 ± 0.2	81 ± 2	0.882
N V	5.25	1238.821	1238.845	9 ± 1	10.7 ± 0.3	80 ± 2	1.557
Si IV	4.8	1393.755	1393.768	6 ± 1	20.2 ± 0.5	75 ± 2	1.320
O IV]	5.2	1401.156	1401.184	9 ± 2	2.7 ± 0.2	49 ± 4	0.802
Si IV	4.8	1402.770	1402.779	5 ± 1	11.3 ± 0.4	77 ± 2	0.915
O IV] (+ S IV])	5.2	1404.806	1404.804	3 ± 6	1.3 ± 0.2	81 ± 11	0.581
O IV]	5.2	1407.386	1407.410	9 ± 7	0.6 ± 0.2	51 ± 13	0.709
Ni II	4.3	1411.071	1411.080	5 ± 3	1.5 ± 0.2	49 ± 4	0.874
Fe II + Ni II + S I	4.3	...	1412.853	...	1.2 ± 0.2	45 ± 6	0.973
Si II	4.3	1533.432	1533.416	0 ± 2	3.3 ± 0.4	45 ± 4	0.883
C IV	5.0	1548.202	1548.232	9 ± 1	52.8 ± 1.0	79 ± 2	0.694
C IV	5.0	1550.774	1550.795	8 ± 1	28.7 ± 0.7	77 ± 2	1.284
Fe II	4.3	1559.084	1559.089	4 ± 2	4.9 ± 0.6	37 ± 4	1.392
Fe II	4.3	1563.788	1563.781	2 ± 2	3.2 ± 0.4	31 ± 4	1.064
He II	4.0[e]	1640.428[e]	1640.429	4 ± 1	7.0 ± 0.5	38 ± 2	1.261
Mg II[d]	4.2	2795.528	2795.500	0 ± 1	2810 ± 50	...	...
Mg II[d]	4.2	2802.705	2802.677	0 ± 1	2310 ± 50	...	...
Two-Gaussian Fits							
N V	5.25	1238.821	1238.842	9 ± 1	6.6 ± 0.9	62 ± 4	0.979
	5.25	1238.821	1238.836	7 ± 4	4.8 ± 0.9	141 ± 16	0.979

[a] Approximate temperature of line formation, based on the peak of the line contribution function.

[b] Line velocity relative to the star, assuming a stellar radial velocity of -3.5 km s^{-1}.

[c] Optical depth at line center was a free parameter of this fit (see § 3.4). The FWHM given in the table is the line width that would have been observed if the line was not opacity-broadened, so this is the line width that should be characteristic of the thermal and turbulent gas motions.

[d] The fluxes and velocities of the Lyα and Mg II lines were measured directly rather than by a Gaussian fit.

[e] The line formation temperature and rest wavelength listed are for the radiative recombination model (see § 3.2).

not seem to have any excess emission at -90 km s^{-1}, so log $T = 4.7$ may represent a lower temperature limit for the blue-wing excess phenomenon. With the strong, uneven continuum under most of Procyon's emission lines, it is tempting to blame the blue-wing excesses on continuum variations and/or line blends, but this does not explain why there are no *red*-wing excesses as well. Therefore, we believe the excess emission in the blue wings of the transition-region lines is due to emission in those lines.

Despite the blue-wing excesses, the line velocities listed in Table 2 demonstrate that the transition-region lines as a whole are *redshifted* with respect to the photosphere. Ayres (1991) also found that Procyon's transition-region lines are redshifted, although his velocities measured from lower quality *IUE* data do not agree particularly well with ours. The line velocities are plotted versus line formation temperature in Figure 6. The line formation temperatures, which are listed in Table 2, are based on the peaks of the line contribution functions (see, e.g., Brown et al. 1984; Linsky et al. 1995b). However, the lines with temperatures listed at and below log $T = 4.7$ are actually formed over a fairly broad range of temperatures. The line formation temperatures we have assumed for these lines may be too high because the density and total mass of emitting material should be higher at lower temperatures, thereby allowing more emission to be produced at lower temperatures than the contribution functions suggest. Nevertheless, Figure 6 demonstrates an obvious increase of line redshift with temperature.

Line redshifts have been observed in the UV spectra of many stars besides Procyon, including the Sun (Ayres et al. 1983; Ayres, Jensen, & Engvold 1988). For the Sun, the redshifts are roughly 10 km s^{-1} near log $T = 5.1$ and decrease to both hotter and cooler temperatures (Doschek, Feldman, & Bohlin 1976; Athay 1988; Achour et al. 1995). The redshifts of Procyon's lines are similar to those observed on the Sun, although we see no evidence for a decrease in line velocity above log $T = 5.0$. It is unlikely that these redshifts represent a net mass downflow. Instead, it is widely believed that we are seeing the effects of a circulation system in which the downward leg of the flow pattern produces most, if not all, of the transition-region line emission. This could occur if the upflowing material is cool but is heated to transition-region temperatures before falling back to the star. Observational evidence for this scenario centers on solar spicules, which are believed to consist of cool material (log $T \sim 4.0$) that has been transported from the chromosphere into the corona. Cheng (1992) demonstrated quantitatively that it is possible that the spicular material is heated to transition-region temperatures before descending back toward the chromosphere, thereby creating the redshifts observed in transition-region lines. UV images of the solar limb in fact show spicular structure at transition-region temperatures as well as chromospheric temperatures (Feldman, Doschek, & Mariska 1979; Cook & Brueckner 1991).

The outwardly directed solar chromospheric jets detected in UV lines of Si II and C I by Dere, Bartoe, & Brueckner (1983) are probably spectral signatures of the spicules. The absence of spatial resolution prevents us from directly determining whether chromospheric jets exist on Procyon. Rather than being blueshifted, Procyon's disk-averaged chromospheric

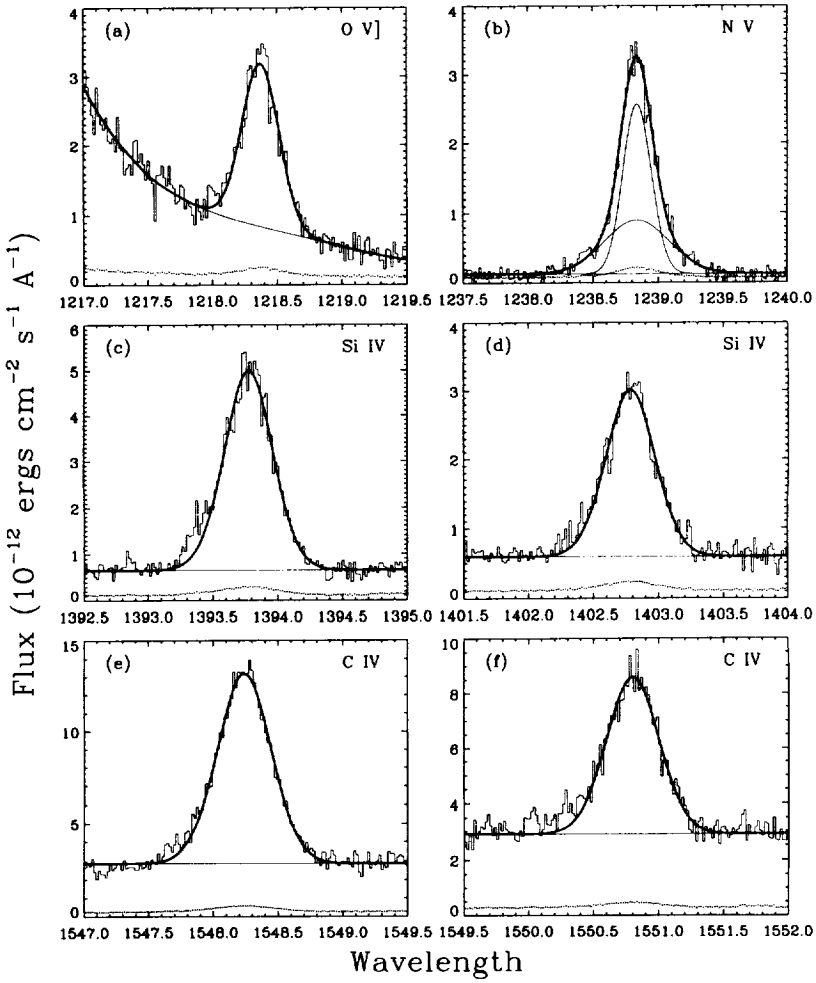

FIG. 4.—Gaussian fits to six of Procyon's strong transition-region lines. The data are displayed in histogram form, and the dots show the 1 σ errors. The fit to the N v λ1239 line is a two-Gaussian fit. The parameters for these fits are listed in Table 2.

lines are either slightly redshifted or show no Doppler shift whatsoever. This by no means precludes the existence of spicular structures on Procyon, however, since the solar chromospheric jets would not be easily detectable in disk-integrated spectra. It is not known whether the mass flows implied by the Mg II h and k line asymmetries seen in the Sun, Procyon (see § 3.5), and other stars are associated with the chromospheric jets and/or spicules (Rutten & Uitenbroek 1991).

Downflowing spicular material is just one possible explanation for the redshifted transition-region lines. In addition to the numerous hypotheses summarized by Brekke (1993), Reale, Peres, & Serio (1995) have recently added another, which attributes the redshifts to downflowing material produced during the evolution of thermal perturbations in the transition region. We also call attention to Mullan & Cheng's (1994) acoustically heated model atmosphere for Procyon, in which they predict that the average particle velocity in the transition region is 2–9 km s^{-1} directed toward the photosphere, which may be consistent with our observed redshifts for the transition-region lines. Mullan & Cheng explain that in their model the material lifted upward by acoustic shocks must eventually come down, but the upwardly directed shocked material should be denser than the downflowing material. The predicted net downdrafts can then be seen as a consequence of mass conservation, which requires $n_u v_u = n_d v_d$, where n_u and v_u are the time-averaged density and velocity of the upflowing material and n_d and v_d are the time-averaged density and velocity of the downflowing material, respectively. Since $n_u > n_d$, v_d should be greater than v_u. However, since the flux in a collisionally excited line is proportional to n^2 and the upflowing material has the higher density, the net downdraft predicted by the model does not necessarily produce a redshifted emission line.

McClymont & Craig (1987), among others, have shown that line redshifts can be produced by steady flows through a magnetic loop that is heated predominantly in one leg. In their model, the portion of the loop that contains downflowing material at transition-region temperatures is much longer than the corresponding section that contains upflowing material, which results in a much larger emission measure for the downflowing leg of the loop. Perhaps the blue-wing excesses we observe in Procyon's transition-region lines could be a signature of the upflowing leg of such a circulation system. Taken at face value, the blue-wing excesses seem to indicate the presence of outbound mass flows with velocities of $\sim$90 km s^{-1}. Such flows would be supersonic since the sound speed at transition-region temperatures is 30–60 km s^{-1}. Outflows such as this are occasionally seen on the Sun during transition-region explo-

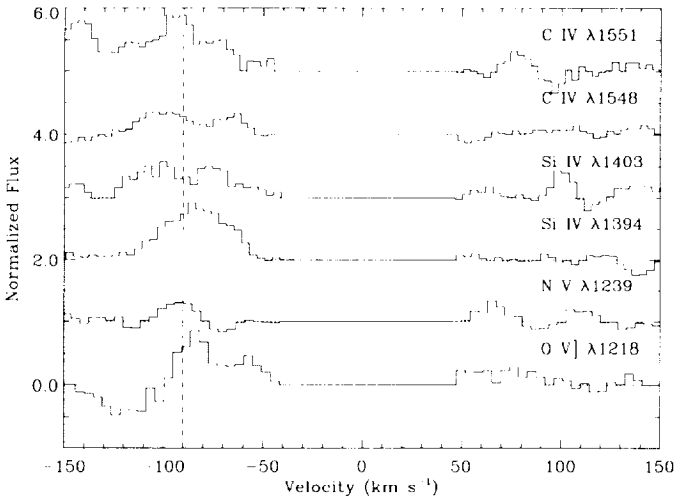

FIG. 5.—Smoothed residuals of the fits in Fig. 4. The horizontal dotted lines are the zero flux levels for the six lines. The residuals at the line centers (-45 km s^{-1} $< v <$ 45 km s^{-1}) have been set to zero to focus attention on the wings. To permit a more equitable comparison of the six emission lines, they were normalized to have the same integrated flux before the residuals were computed. Procyon's transition-region lines all seem to have excess flux at about -90 km s^{-1} (*dashed line*). There does not seem to be a corresponding flux excess in the red wing.

sive events (see, e.g., the "jets" discussed by Brueckner & Bartoe 1983). However, the blue-wing excesses of Procyon's disk- and time-averaged transition-region line profiles seem to be localized to the blue wings of the emission lines, whereas a turbulent phenomenon like the explosive events should affect the entire profile and presumably produce emission in the red wing as well, as discussed in § 3.1. Therefore, we are not sure if there is a true solar analog for Procyon's blue-wing excess phenomenon.

Two very different line formation mechanisms have been proposed for the He II λ1640 multiplet, which imply very different line formation temperatures (see, e.g., Feldman et al. 1975). The collisional excitation model predicts that He II is formed at log $T \sim 5.0$, whereas the radiative recombination model predicts line formation at lower temperatures near log $T \sim 4.0$.

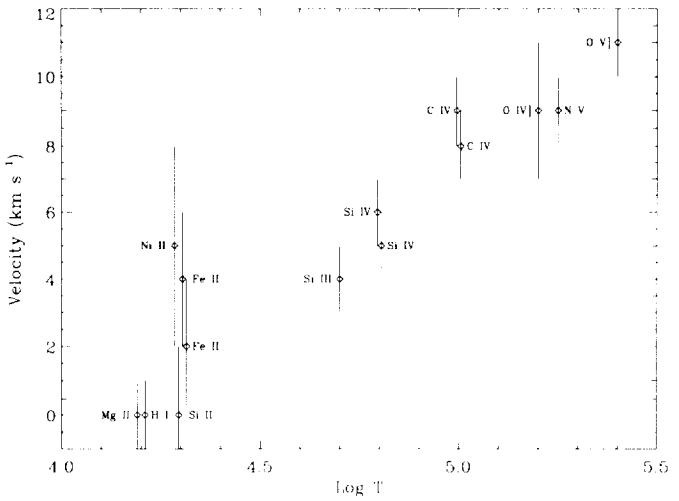

FIG. 6.—Line redshifts for Procyon as a function of line formation temperature.

For Procyon, the width of the He II line is similar to that of the Fe II, Si II, and Ni II lines, and if we use the centroid wavelength of the radiative recombination model (1640.428 Å) as the rest wavelength of the line, the resulting line velocity, $v = +4$ km s^{-1}, is also consistent with those of the Fe II, Si II, and Ni II lines. If we had instead used the centroid wavelength of the collisional excitation model (1640.438 Å), the line velocity would have been 1 km s^{-1}, which is *not* consistent with the velocities of the lines formed at log $T \sim 5.0$. Therefore, we believe that the He II multiplet is mostly formed at chromospheric temperatures on Procyon. Wahlstrøm & Carlsson (1994) demonstrated that this is also the case on the Sun. In the radiative recombination model, energetic radiation from the corona ionizes helium atoms, which then produce the He II λ1640 emission through recombination. In the bandpass of the *Einstein* IPC, the X-ray flux of Procyon is $f_{\rm IPC} = 9 \times 10^{-12}$ ergs cm^{-2} s^{-1} (Wood et al. 1994), which means that $f_{\rm IPC}/f_{\rm He\,II} = 13$ for Procyon. Hartmann, Dupree, & Raymond (1982) predicted that $f_{\rm IPC}/f_{\rm He\,II} \sim 30$ for the radiative recombination model of He II line formation. This prediction is too high by about a factor of 2, but the uncertainty in the theoretical $f_{\rm IPC}/f_{\rm He\,II}$ ratio is surely quite large.

3.3. *Electron Density of the Transition Region*

The electron density is one of the fundamental physical parameters that must be measured or estimated before a model of a stellar atmosphere can be calculated. Spectral density diagnostics are therefore of crucial importance. In UV spectra, all such diagnostics rely on density-sensitive line ratios, which include optically thin intersystem lines such as the O V] λ1218 and O IV] λ1400 multiplet lines we have observed in our Procyon spectra. Unfortunately, the continuum in the 1880–1920 Å region proved to be too strong to detect the Si III] λ1892 and C III] λ1909 lines (see Fig. 1).

The 1395–1410 Å spectral region contains four O IV] lines that were detected in the GHRS spectra of Capella. The flux ratios of these O IV] lines are the most accurate diagnostics available in our spectra for determining transition-region densities (Linsky et al. 1995b). The strongest O IV] line at 1401.156 Å is obviously detected in our spectra, but the weaker lines are difficult to see. We have smoothed the 1380–1420 Å spectrum in Figure 1 to try to reveal these lines. There appears to be a feature near 1400 Å that could be the O IV] λ1399.8 line, but the large width of the feature suggests that it is likely blended, so we have not listed this feature in Table 2. For similar reasons the feature at 1406 Å, which could be the S IV] λ1406.1 line, has also not been listed in Table 2. The possible detection of S IV] λ1406 means that the weaker S IV] line at 1404.8 Å may be blended with the O IV] line we have identified at that wavelength. However, the calculations of Cook et al. (1995) demonstrate that the O IV] line should still account for at least 75% of the flux in the feature, even if the feature at 1406 Å is entirely S IV] λ1406, so we have identified the line as O IV] λ1405 and listed the flux of this line in Table 2. The O IV] line at 1407.4 Å is visible, but it is barely a 3 σ detection. Note that the O IV] λ1399.8 line should have the same flux as the line at 1407.4 Å (Cook et al. 1995).

The electron density can now be estimated from the observed flux ratios of the O IV] lines listed in Table 2 and an atomic model of O IV] (Cook et al. 1995). Unfortunately, the errors in the fluxes of the weaker O IV] lines are high because of the possible S IV] blend in the 1405 Å line and low signal-to-noise ratios in all the lines. The flux ratios seem to indicate

densities in the neighborhood of 10^{10} cm^{-3}. However, this density is not too far from the lower limit where the flux ratio versus density relations flatten, so when the large errors in the flux ratios are taken into consideration we find we can only quote an upper limit for the electron density of $\log n_e < 10.3$. This provides an upper limit for the transition-region pressure (in units of cm^{-3} K) of $\log P_e < 15.5$.

Using Fe XIX lines observed by *EUVE*, Schmitt, Haisch, & Drake (1994) measured a coronal density for Procyon of $\log n_e = 9.70 \pm 0.15$ at a temperature of $\log T = 6.3$. The implied coronal pressure is $\log P_e = 16.00 \pm 0.15$, which is significantly higher than our upper limit for the pressure in Procyon's transition region. The interpretation of *IUE* and X-ray data presented by Jordan et al. (1986) suggested a similar pressure difference between the transition region and corona. This pressure difference is inconsistent with a simple, spherically symmetric, one-dimensional atmosphere in hydrostatic equilibrium and instead suggests that Procyon's transition-region emission is not uniformly distributed on the stellar surface. Jordan et al. (1986) proposed that this could imply supergranulation structures on Procyon similar to those seen on the Sun, where most of the emission is produced at the cell boundaries. Feldman & Laming (1994) showed that, in general, no physical connection appears to exist between the solar transition region and the solar corona. If this is true on Procyon as well, then the pressures in the transition region and corona should not be expected to be consistent with hydrostatic equilibrium.

3.4. *Line Widths and Opacities*

The weighted average width of the emission lines formed at temperatures above $\log T = 4.6$ is FWHM $= 77.6 \pm 2.0$ km s^{-1}, where the quoted error is the standard deviation of the mean. The O IV] λ1401 and λ1407 lines are the only transition-region lines that have widths that seem discrepant, as these lines are significantly narrower than the other transition-region lines. It is unclear exactly why the O IV] line widths are discrepant, but we note that the width of the O IV] lines is similar to that of the narrow component of the N V line, which is formed at essentially the same temperature as O IV]. Perhaps O IV] emission in the broad component is inhibited by high densities, as is suggested in § 3.1 for the O V] line. If the O IV] lines are ignored, the mean line width becomes FWHM $= 78.7 \pm 0.9$ km s^{-1}. The chromospheric Ni II, Fe II, Si II, and He II lines are much narrower, with an average width of FWHM $= 39.6 \pm 2.3$ km s^{-1}. Rotational broadening makes little contribution to these widths since $v \sin i$ is only 3.6 km s^{-1} (Gray 1982). The nonthermal velocities present in the transition region and chromosphere can be estimated for optically thin lines using the equation (in cgs units)

$$\left(\frac{\Delta\lambda}{\lambda}\right)^2 = 3.08 \times 10^{-21}\left(\frac{2kT}{m_i} + \xi^2\right), \quad (1)$$

where $\Delta\lambda$ is the FWHM, T is the line formation temperature, m_i is the ion mass, and ξ is the "most probable" nonthermal speed. Using this equation, we find that $\xi = 46.1 \pm 0.5$ km s^{-1} for the transition-region lines (excluding O IV]) and $\xi = 22.7 \pm 1.6$ km s^{-1} for the chromospheric lines. These velocities are significantly higher than the solar values: $\xi \approx 25$ km s^{-1} for solar transition-region lines and $\xi \approx 15$ km s^{-1} for solar chromospheric lines (Dere & Mason 1993). The hydrodynamic models of Nordlund & Dravins (1990) suggest that convective motions should be more vigorous and should penetrate to higher altitudes on Procyon than on the solar-like G2 V star α Cen A. These properties of convection on Procyon might explain why Procyon has broader emission lines than the Sun.

These estimates of the nonthermal velocities are accurate only if the lines are not significantly opacity-broadened. Only the Lyα and Si III λ1207 lines of Procyon have profiles that are noticeably affected by opacity (see below). The stronger C IV line should have twice the opacity of the weaker line, so if the lines were optically thick the stronger line should be broader. The excellent agreement between the widths of the stronger and weaker C IV lines suggests that either these lines are not optically thick or that macroturbulence is masking the opacity effects. The same is true for the two Si IV lines, the widths of which are also in agreement. On the other hand, the C IV λ1548/λ1551 and Si IV λ1394/λ1403 flux ratios suggest the presence of some detectable opacity in these lines. Since the ratio of collisional excitation rates for the C IV and Si IV multiplets is 2.0 and these lines do not share a common upper level, the flux ratios should be 2.0 if the C IV and Si IV lines are optically thin or effectively thin. Instead, we find that these ratios are close to 1.8, similar to the ratios found for AU Mic (Linsky & Wood 1994) and Capella (Linsky et al. 1995b) but different from the Sun's line ratios, which *are* close to 2.0 (Dere et al. 1987).

As previously stated, the Si III λ1207 line has a profile that we believe is opacity-broadened. Figure 7*a* shows a single-Gaussian fit to the Si III line. The Gaussian is not a particularly good fit ($\chi^2_\nu = 2.201$), because the top of the observed profile is

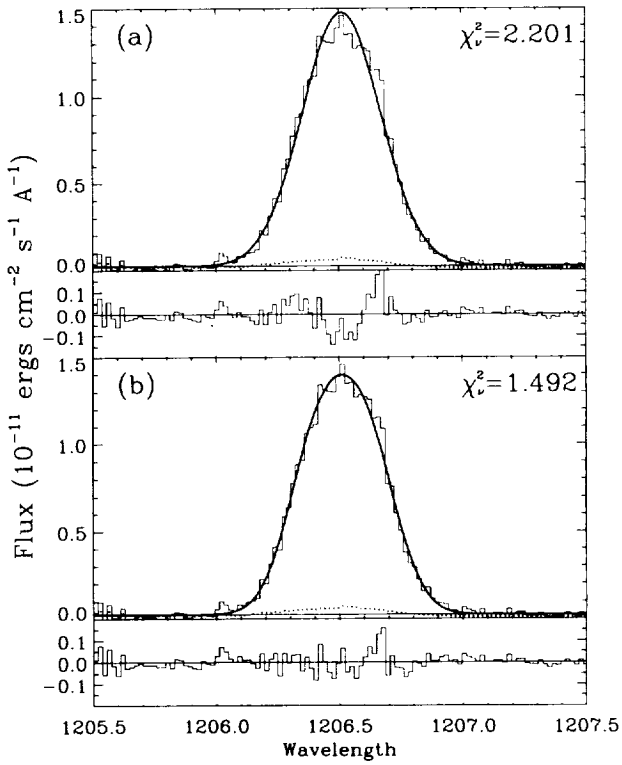

FIG. 7.—(*a*) Single-Gaussian fit to the Si III λ1207 line of Procyon with the residuals of the fit below. The data are displayed in histogram form, and the dots show the 1 σ errors. The χ^2_ν value is a measure of the quality of the fit. (*b*) Same as (*a*), but the optical depth has been included as a free parameter of the fit (see § 3.4). The χ^2_ν value is lower than in (*a*), indicating a much better fit. This illustrates that the non-Gaussian nature of the line can be explained by opacity broadening.

more rounded and less pointed than the Gaussian. To demonstrate that the non-Gaussian shape of the Si III line can be explained by opacity broadening, we have used the following technique to perform another fit to the line in which the line-center optical depth is a fourth free parameter.

The formal solution to the radiative transfer equation is

$$I_\nu(\tau = 0, \mu) = \frac{1}{\mu}\int_0^{\tau_\nu} S_\nu(t)e^{-t/\mu}\,dt\ . \quad (2)$$

If ϕ_ν is the line profile function, the optical depth at line center is $\tau_o = (\phi_o/\phi_\nu)\tau_\nu$. In order to consider the optical depth as a free parameter of our profile-fitting routine, we first had to assume a functional form for the source function $S_\nu(t)$. We chose to use an Eddington-Barbier relation of the form $S_\nu(t) = a + bt$ with $a = 1$ and $b = \phi_o/\phi_\nu$. Equation (2) can be solved numerically by using a quadrature sum (Mihalas 1978). For a one-point Gaussian quadrature, $\mu = 1/3^{1/2}$. With these assumptions, equation (2) becomes

$$I_\nu = \sqrt{3}\int_0^{\tau_\nu}\left(1 + \frac{\phi_o}{\phi_\nu}t\right)e^{-\sqrt{3}t}\,dt\ . \quad (3)$$

This equation can be solved analytically to yield

$$I_\nu(\tau_o) = N\left[1 + \frac{1}{\sqrt{3}}\frac{\phi_o}{\phi_\nu} - \exp\left(-\sqrt{3}\tau_o\frac{\phi_\nu}{\phi_o}\right)\left(1 + \tau_o + \frac{1}{\sqrt{3}}\frac{\phi_o}{\phi_\nu}\right)\right], \quad (4)$$

where N is a factor we use to normalize the computed profile to the observed profile. This is the equation we used to obtain the fit in Figure 7*b*.

The fit shown in Figure 7*b* is a significant improvement over that shown in Figure 7*a*. This is not an acceptable 2 σ fit, however, mostly due to excess emission on the red shoulder of the line, which may represent a real asymmetry in the line profile. The Si III line width listed in Table 2, FWHM = 81 km s^{-1}, is the width that would have been observed if there were no opacity broadening. For comparison, the width of the Gaussian in Figure 7*a* is FWHM = 92 km s^{-1}, illustrating the degree to which opacity has broadened the line. Removal of opacity broadening leads to an intrinsic width (81 km s^{-1}) that is consistent with the widths of the other transition-region lines. Despite the uncertainties present in our analysis, the fit in Figure 7*b* illustrates that the non-Gaussian nature of the Si III line can be explained by opacity broadening.

The optical depth we derive for Si III λ1207 is $\tau_o = 0.7$, but this optical depth is highly uncertain. The Eddington-Barbier relation we used to model the source function is more appropriate for emission in an extended atmosphere. However, a slab geometry is more appropriate for transition-region lines, since they are emitted in a relatively thin atmospheric layer. The source function of a transition-region line should increase with depth initially but should reach a maximum near the center of the emission layer and then decline until the bottom of the layer is reached. We experimented with schematic source functions that have this property and found that these source functions suggested somewhat higher optical depths for the Si III line.

Another possible problem with equation (4) is that it implicitly assumes that the Doppler broadening is due entirely to microturbulence rather than macroturbulence. The line opacity is dependent on the former but not on the latter. Macroturbulence can be included as a fit parameter by convolving the profile given by equation (4) with a Gaussian, where the width of the Gaussian is the fifth parameter of the fit. This assumes, however, that the macroturbulence does in fact have a Gaussian velocity distribution, which is by no means certain. We tried fitting the Si III line with such a profile model and found that the inclusion of macroturbulence did not improve the quality of the fit. Since macroturbulence gives a profile a more Gaussian shape, it can hide the effects that opacity has on the line profile. Therefore, if macroturbulence is present in the Si III line, the line's optical depth will be larger than the $\tau_o = 0.7$ value we derived. At the very least, the $\tau_o = 0.7$ result should be a solid lower limit to the actual optical depth, since the use of an accurate source function and a correction for any macroturbulence present would result in a larger derived optical depth.

The optical depth of a line and the line's surface flux are related by the equation

$$\frac{\tau_o}{F} = \frac{9.7\times10^{-8}gf\lambda^3T^{3/2}}{\Omega\Delta\lambda P_e}\exp\left(\frac{1.44\times10^8}{\lambda T}\right), \quad (5)$$

where $\Delta\lambda$ is the FWHM of the line (after correcting for opacity broadening) and P_e is the electron pressure in units of cm^{-3} K. Both λ and $\Delta\lambda$ are in angstroms. Brown & Jordan (1981) derived this equation in terms of a Gaunt factor, but we express it in terms of the statistical weight of the lower atomic level g, the oscillator absorption strength f, and the collision strength Ω. The line fluxes in Table 2 can be converted to stellar surface fluxes by using the stellar radius and distance listed for Procyon in § 1, although one must make the assumption that the emission is produced uniformly over the stellar surface. We can then solve for the electron pressure in equation (5) since we have an estimate of the optical depth of the Si III λ1206 line and all other quantities are known for that line. For the Si III line, $\Omega = 7.5$ (Dufton & Kingston 1989), $g = 1$, and $f = 1.669$ (Morton 1991). We therefore find that $P_e = 7.0\times10^{14}$ cm^{-3} K at log $T = 4.7$, where the Si III line is formed. If $\tau_o = 0.7$ is considered to be only a lower limit, then the pressure is an upper limit (log $P_e < 14.8$) that is significantly lower than the upper limit for the pressure derived in § 3.3 by using the O IV] lines (log $P_e < 15.5$).

3.5. *The* Mg II *h and k Lines*

The Mg II h and k lines with rest wavelengths in air of 2802.705 and 2795.528 Å, respectively, are shown in Figure 3. For Procyon, the chromospheric Mg II h and k emission features are both located at the center of very broad absorption lines produced by photospheric Mg II absorption. The much narrower chromospheric emission lines at the bottom of these absorption troughs are self-reversed because of the large optical depth of the Mg II–emitting region. Brown & Jordan (1981) estimated an optical depth of order $\tau_o = 5000$ for the k line, based on *IUE* observations and the atmospheric model of Ayres, Linsky, & Shine (1974). Very narrow interstellar absorption features are seen near the center of both Mg II lines. Thanks to the high resolution of the echelle-B grating, these interstellar features are easily separable from the central reversals of the stellar emission lines, and an analysis of the interstellar absorption has been made by Linsky et al. (1995a).

The blue emission peaks of the self-reversed Mg II lines are significantly stronger than the red peaks. A similar asymmetry is seen for disk-averaged solar Mg II lines (Donnelly, White, & Livingston 1994). Solar Ca II H and K lines, which are similar

to the Mg II h and k lines in many respects and show the same asymmetry, have been studied extensively with ground-based observations. Spatially resolved solar observations of the Ca II lines generally do not resemble the disk-averaged profiles. In active regions, the emission is strong but relatively symmetric. Asymmetric line profiles with stronger blue peaks are more typically observed in quiet regions of the chromosphere, where there are many small, bright points of Ca II emission scattered over the solar disk. Most, but not all, of the Ca II profiles observed from these "cell grains" show emission almost entirely in the blue peak. Rutten & Uitenbroek (1991) gave a thorough review of the observations and models of the solar Ca II H and K cell grains. The cell grains typically have lifetimes of a few minutes and often exhibit an oscillatory behavior that appears to originate in the photosphere. It seems likely, therefore, that the stronger Ca II and Mg II blue peaks seen in the disk-averaged spectra of both Procyon and the Sun are signatures of hydrodynamical processes in the chromospheres of these two stars.

Since the Mg II line profiles are controlled by opacity and atmospheric structure rather than by turbulence, we do not try to fit Gaussians to Procyon's Mg II lines, but we do estimate velocities and fluxes for these lines (see Table 2). Inspection of the sides of the emission lines reveals no significant Doppler shifts. The Mg II subordinate line at 2798.0 Å, which is seen in absorption, also appears to be centered in the stellar rest frame. The interstellar absorption features were removed before computing line fluxes. The flux of the k line was measured between the k_1 minima at roughly 2794.8 and 2796.2 Å, and the flux of the h line was measured between the h_1 minima near 2802.0 and 2803.2 Å.

When measuring the Mg II fluxes, one can assume a flat continuum extrapolated between the k_1 and h_1 minima (at about 9.5×10^{-11} ergs cm^{-2} s^{-1} Å^{-1} and 1.15×10^{-10} ergs cm^{-2} s^{-1} Å^{-1}, respectively), or one can simply assume that there is no photospheric continuum under the chromospheric emission lines. We used the latter assumption in the computation of the Mg II fluxes listed in Table 3 because the Mg II ions in the photosphere and/or lower chromosphere should absorb essentially all of the continuum photons near line center, where the chromospheric emission lines are located (Linsky & Ayres 1978). If we had instead extrapolated a flat continuum between

TABLE 3

LINE PROFILE PARAMETERS FOR HR 1099

Ion	log T[a]	λ_{rest} (Å)	λ_{meas} (Å)	v[b] (km s^{-1})	f (10^{-13})	FWHM (km s^{-1})	χ^2_ν
Single-Gaussian Fits							
Si III	4.7	1206.510	1206.611	-9 ± 2	8.7 ± 0.3	167 ± 5	1.105
H I[c]	4.2	1215.670	1215.821	3 ± 3	1200 ± 200	...	...
O V]	5.4	1218.344	1218.437	-11 ± 12	1.8 ± 0.3	160 ± 22	1.121
N V	5.25	1238.821	1238.957	-1 ± 3	2.8 ± 0.1	124 ± 5	0.978
Si IV	4.8	1393.755	1393.520	8 ± 2	5.5 ± 0.1	179 ± 4	1.215
O IV]	5.2	1399.774	1399.507	1 ± 13	0.15 ± 0.02	201 ± 24	1.048
O IV]	5.2	1401.156	1400.889	1 ± 6	0.76 ± 0.06	201 ± 24	1.048
Si IV	4.8	1402.770	1402.516	4 ± 3	2.7 ± 0.1	175 ± 4	1.048
O IV]	5.2	1404.806	1404.539	1 ± 13	0.27 ± 0.04	201 ± 24	1.048
O IV]	5.2	1407.386	1407.119	1 ± 13	0.16 ± 0.02	201 ± 24	1.048
Si II	4.3	1533.432	1533.208	13 ± 5	0.70 ± 0.06	147 ± 10	0.962
C IV	5.0	1548.202	1547.949	8 ± 1	26.6 ± 0.4	194 ± 2	2.677
C IV	5.0	1550.774	1550.521	8 ± 1	13.6 ± 0.3	178 ± 2	2.677
C I	3.8	1561 mult.	...	...	2.8 ± 0.1	...	...
He II	4.0[d]	1640.428[d]	1640.155	5 ± 1	19.4 ± 0.3	154 ± 2	2.564
C I[e]	3.8	1656.267	1656.002	7 ± 1	2.2 ± 0.1	49 ± 7	1.375
C I[e]	3.8	1657 mult.	...	...	10.5 ± 0.2	...	...
O III]	4.9	1666.153	1665.895	9 ± 8	1.2 ± 0.1	209 ± 14	0.956
Al II	4.3	1670.787	1670.560	14 ± 4	2.5 ± 0.1	185 ± 7	1.156
Si III]	4.6	1892.030	1891.693	0 ± 4	2.5 ± 0.1	160 ± 6	1.135
S I	3.8	1900.286	1899.940	-2 ± 5	0.50 ± 0.09	54 ± 8	1.047
C III]	4.8	1908.734	1908.231	-26 ± 4	2.8 ± 0.1	203 ± 8	1.233
S I	3.8	1914.698	1914.392	5 ± 6	0.30 ± 0.08	53 ± 11	1.024
Two-Gaussian Fits							
Si IV	4.8	1393.755	1393.513	6 ± 2	2.5 ± 0.8	117 ± 20	1.042
	4.8	1393.755	1393.513	6 ± 2	3.1 ± 0.8	240 ± 36	1.042
C IV	5.0	1548.202	1547.965	11 ± 1	9.6 ± 0.6	82 ± 5	1.137
	5.0	1548.202	1547.927	3 ± 2	18.4 ± 0.7	250 ± 4	1.137
C IV	5.0	1550.774	1550.537	11 ± 1	4.8 ± 0.3	82 ± 5	1.137
	5.0	1550.774	1550.499	3 ± 2	9.2 ± 0.3	250 ± 4	1.137
He II	4.0[d]	1640.428[d]	1640.185	11 ± 1	7.0 ± 0.6	52 ± 7	1.120
	4.0[d]	1640.428[d]	1640.119	-2 ± 2	13.4 ± 0.5	204 ± 5	1.120
C III] + ?	4.8	1908.734	1908.396	0	2.1 ± 0.2	187 ± 15	1.046
	?	?	1907.795	?	0.7 ± 0.2	101 ± 26	1.046

[a] Approximate temperature of line formation, based on the peak of the line contribution function.

[b] The line velocity relative to the K1 star.

[c] The flux and velocity of Lyα were measured directly rather than by a Gaussian fit.

[d] The line formation temperature and rest wavelength listed are for the radiative recombination model (see § 4.2).

[e] The C I λ1656.3 line is the only resolvable member of the λ1657 multiplet.

the k_1 and h_1 minima, the fluxes of the h and k lines would have been 8.87×10^{-11} and 1.48×10^{-10} ergs cm^{-2} s^{-1}, respectively. However, the h and k lines have different profiles if we assume such a continuum since the h line would appear to have a deeper central reversal and a larger blue/red peak ratio than the k line. On the other hand, the h and k line profiles have essentially the same shape if one assumes a zero continuum level for both lines. This is empirical evidence in favor of this assumption, since the h and k lines of most stars, including Capella (Linsky et al. 1995b) and HR 1099, appear to be nearly identical if the flux and width of the h line are slightly increased.

4. ANALYSIS OF HR 1099 DATA

4.1. *Line Profile Parameters and the Search for Broad Components*

The first step in analyzing the HR 1099 data was to determine which of HR 1099's two stars is responsible for the binary's emission lines. By analyzing *IUE* spectra at different orbital phases, Ayres & Linsky (1982) found that the K1 star accounts for most of the emission. Our data not only confirm this finding but also suggest that the G5 star's flux contribution is truly negligible in many of the strongest emission lines observed with the moderate-resolution gratings (e.g., C IV, Si IV, and He II). Both the near-symmetric appearance of these lines and the good agreement of the line velocities with the rest frame of the K1 star support this conclusion. The only lines in which the presence of the G5 star is obvious are the Mg II h and k lines, but even for those lines the G5 star accounts for only $\sim$7.5% of the line flux (as will be discussed in § 4.5). For the C IV, Si IV, and He II lines, we believe the G5 star's contribution must be only $\sim$5% at most. Any larger contribution should have been detected because our observations were taken at or near quadrature when the velocity separation between the two stars is near the maximum of 111.1 km s^{-1}.

We fit Gaussians to all of HR 1099's emission lines, as we did for the Procyon data, and Table 3 lists the results. We corrected for the instrumental broadening and also corrected for rotational broadening by convolving proposed Gaussian fits with both the instrumental and rotational broadening profiles before testing the fits. This required knowledge of $v \sin i$ for the stars in the HR 1099 system; $v \sin i = 38$ km s^{-1} for the K1 star, and $v \sin i = 13$ km s^{-1} for the G5 star (Vogt & Penrod 1983). (This latter value was required only for the analysis of the Mg II lines in § 4.5.) An example of the instrumental and rotational broadening profiles is shown in Figure 8 for the G160M spectra.

As was the case for Procyon, the Lyα line was not fit with a Gaussian, but its velocity was estimated from parts of the line profile uncontaminated by interstellar absorption. In another paper, this emission line and the superimposed interstellar H I and D I absorption features will be analyzed in the same way as the Lyα lines of Capella and Procyon (Linsky et al. 1993, 1995a), and this analysis will provide an estimate for the amount of stellar Lyα flux that has been removed by the interstellar absorption. For now, we use a cruder estimate based on the Capella and Procyon work, in which it was found that interstellar absorption removed about 60% and 50% of the Lyα line flux for Capella and Procyon, respectively. We expect a similar value for HR 1099 and have therefore assumed a similar correction to estimate the intrinsic stellar Lyα flux in Table 3. The only C I line that is resolvable from either of the

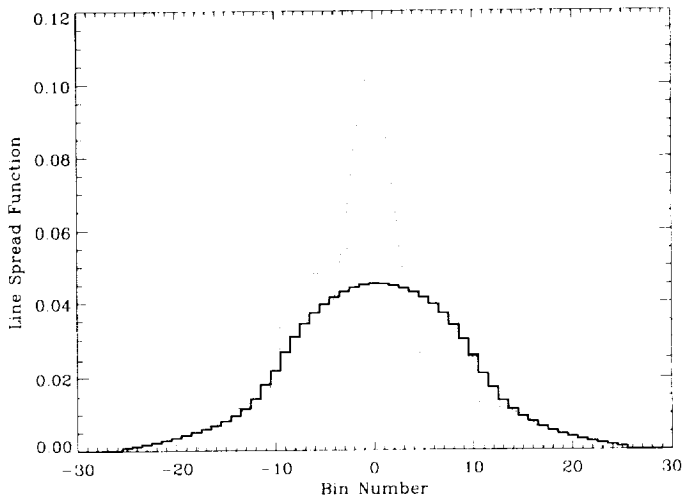

FIG. 8.—Instrumental profile for the G160M grating (Gilliland & Hulbert 1993). The profile is shown as a smooth dotted line, and the rotational broadening profile for HR 1099's K1 star (assuming $v \sin i = 38$ km s^{-1}) is the dotted histogram. The final line-spread function (*solid histogram*) for the G160M observations of HR 1099's K1 star is the convolution of these two profiles.

C I multiplets at 1561 and 1657 Å is the C I λ1656.267 line. The line parameters for this line are listed in Table 3, and the fluxes for the C I λ1561 and λ1657 multiplets are also listed.

Based on the χ^2_ν values in Table 3, the single-Gaussian fits to five of HR 1099's strongest emission lines are not acceptable within the 2 σ criterion. Four of these lines (Si IV λ1394, C IV $\lambda\lambda$1548, 1551, and He II λ1640) have broad wings that we interpret to be indicative of "broad components" similar to those found for AU Mic and Capella. These four lines have therefore been fit with two Gaussians, and Monte Carlo simulations were used to estimate the 1 σ errors in the fit parameters. The results are shown in Figure 9 and in Table 3. The fifth non-Gaussian line, C III] λ1909, was also fit with two Gaussians (see Fig. 9*d* and Table 3), but the interpretation of the C III] line profile is completely different from that of the four line profiles modeled with narrow and broad Gaussian components (see § 4.2).

The C IV λ1548/λ1551 flux ratio is exactly 2.0, the optically and effectively thin limit, and the two C IV lines have almost exactly the same profile. Therefore, we fit the two C IV lines simultaneously and forced the λ1548/λ1551 flux ratio to be 2.0 for both the broad and narrow components, and we forced the widths and velocities of the two components to be the same for both C IV lines. The single-Gaussian fit to the Si IV λ1394 line falls just short of being a 2 σ fit. To reduce the number of free parameters for the two-Gaussian fit to that line, we required the broad and narrow components to have the same velocity. When we tried to do that for the C IV and He II lines (for which the single-Gaussian fits are not even close to being acceptable), we could not obtain 2 σ fits. Therefore, the velocities of the narrow and broad components were allowed to be different for those lines.

We cannot rule out the possibility that HR 1099's weaker lines also have broad components that were not detected statistically because of low signal-to-noise ratio. Figure 10 shows that when these weaker lines are smoothed, many of them do in fact seem to show evidence for non-Gaussian profiles. Compared to the single-Gaussian fits, the smoothed profiles of N V λ1239, Al II λ1671, and Si III] λ1892 seem to have excess flux at

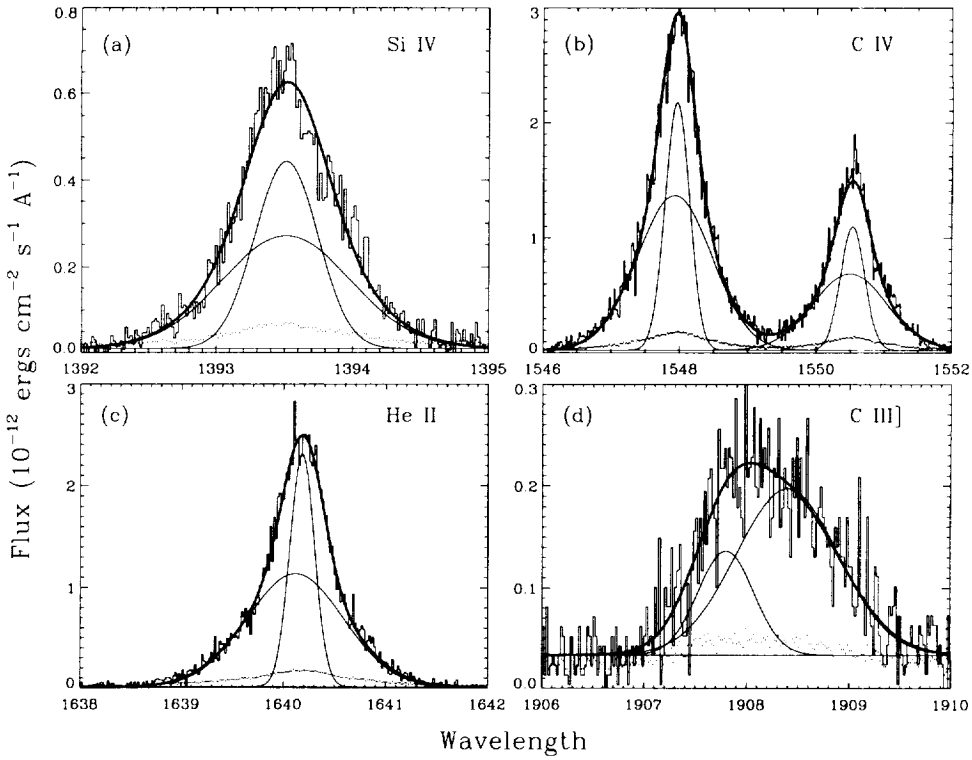

FIG. 9.—Two-Gaussian fits to four lines of HR 1099 that were not well fit with single Gaussians. The data are displayed in histogram form, and the dots show the 1 σ errors. For each fit, the Gaussian components are shown as thin solid lines, and the thick solid line is the convolution of the sum of these Gaussians with both the instrumental and rotational broadening profiles (see Fig. 8). The Si IV, C IV, and He II lines were fit with a narrow component and a broad component. The stronger component of the fit to the C III] feature was forced to be centered in the rest frame of the star. We believe that this component represents the actual "quiescent" C III] emission from HR 1099. The weaker component may represent blueshifted C III] emission produced by some transient event, or it may represent a blend. The parameters for all these fits are listed in Table 3.

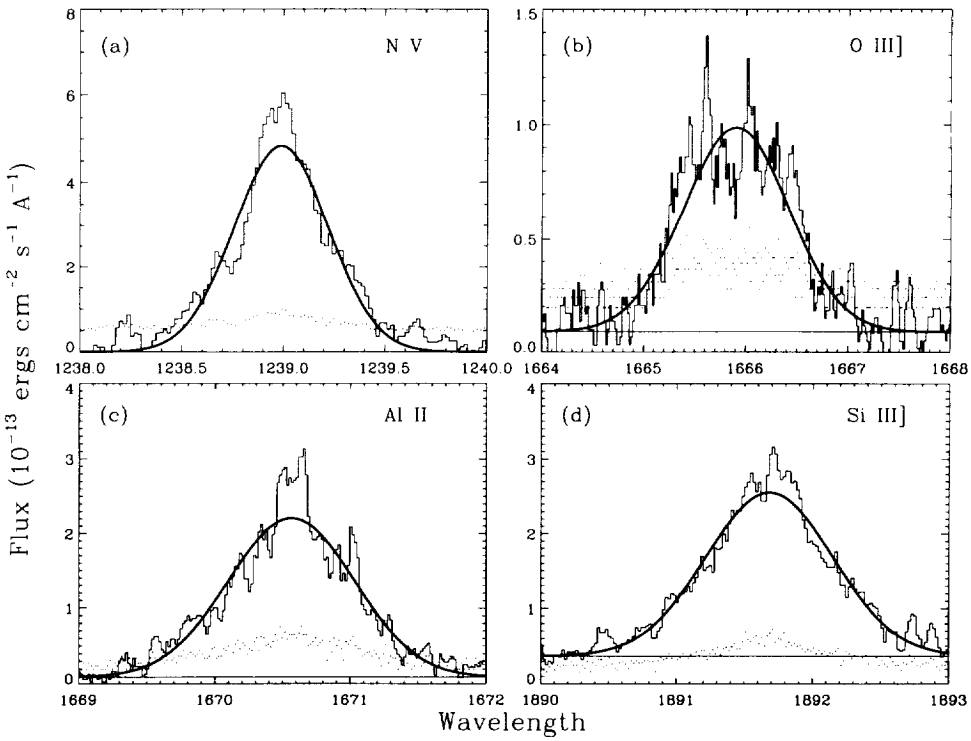

FIG. 10.—Smoothed profiles of four of HR 1099's UV emission lines and the single-Gaussian fits to the lines. The data are displayed in histogram form, and the dots show the 1 σ errors. Although these fits are statistically acceptable, smoothing the profiles seems to reveal some non-Gaussian behavior in all these lines. N V, Al II, and Si III] show at least some evidence for excess flux at line center and in the line wings, which may indicate the presence of broad components such as those found for Si IV, C IV, and He II (see Fig. 9). The O III] line has a strange, boxlike appearance.

line center and in the line wings, which may indicate a shape like that of the C IV and He II lines. We do not feel justified in fitting these lines with two Gaussians, however, since the single-Gaussian fits are statistically acceptable. We do not have an explanation for the strange, boxlike appearance of the O III] λ1666 line in Figure 10*b*.

The broad components of the transition-region lines of AU Mic and Capella account for roughly 40% of the line flux (Linsky & Wood 1994; Linsky et al. 1995b). In contrast, the broad components of HR 1099's lines actually dominate the line flux. The weighted average contribution of the broad component to the total line flux is 65.6% $\pm$ 1.0% for the four lines in which the broad component was detected. This dominance is consistent with the hypothesis that microflares are responsible for the broad components because HR 1099's K1 star is even more active than AU Mic and Capella's G1 star on the basis of the X-ray and UV emission-line surface fluxes of these stars.

We note that magnetic broadening (i.e., Zeeman splitting) and collisional broadening (i.e., Stark and Van der Waals broadening) are almost certainly not responsible for the large transition-region line widths. A magnetic field of order 10^6 G (Brueckner et al. 1988) is necessary to produce lines as broad as those of HR 1099, which seems extreme. The line profiles show no double-peaked structure that would indicate Zeeman splitting, and even though rotational broadening could help hide such structure, the profile of a magnetically broadened transition-region line should still look different than the line profiles that we observe. Brueckner et al. (1988) pointed out that a magnetically broadened C IV λ1551 line should be broader than the C IV λ1548 line, which is not observed for HR 1099 or for any other star that we know of. They also point out that for the Stark effect to become detectable densities must be at least 10^{17} cm^{-3}, which is much higher than the densities of 10^{10}–10^{11} cm^{-3} typically found in stellar transition regions, including that of HR 1099 (see § 4.3 and Byrne et al. 1987). Van der Waals broadening is certainly negligible because transition-region plasmas are almost completely ionized, meaning there are essentially no neutrals available to produce this type of line broadening.

The broad components of HR 1099's C IV and He II lines are significantly blueshifted with respect to the narrow components. This is equivalent to saying that the blue wings of these lines are noticably stronger than the red wings. Linsky et al. (1995b) noted a similar phenomenon in many of the transition-region lines of Capella. The G5 star of HR 1099 cannot account for this effect since any emission from that star would be on the *red* side of the observed C IV and He II lines for the orbital phase of those observations and would therefore produce a stronger red wing rather than a stronger blue wing.

Individual solar transition-region explosive events produce a wide variety of line profiles; some with particularly strong blue wings, some with particularly strong red wings, and some with roughly symmetric wing emission. However, Dere et al. (1989) found that line profiles with dominant blue wings are produced more often than profiles with dominant red wings. Thus, a disk-averaged solar transition-region line profile should have a blueshifted "broad component," which is what is also observed for Capella and HR 1099.

4.2. *Line Velocities*

The velocities listed in Table 3 are all relative to the rest frame of the K1 star, which is given by the equation $v = -15.0 + 49.4 \sin 2\pi\phi$, where ϕ is the orbital phase of the observation (see Table 1). The rest frame of the G5 star is $v = -15.0 - 61.7 \sin 2\pi\phi$ (Fekel 1983). It is difficult to discuss the line velocities of HR 1099 in the same detail as we discussed those of Procyon because the uncertainties in the velocities of many of HR 1099's lines are larger than was the case for Procyon, because of the larger widths and lower signal-to-noise ratios of the lines. Also, the small flux contributions of the G5 star may be affecting the measured line velocities. Even if the G5 star accounts for only a few percent of the fluxes of the emission lines, that is enough of a contribution to produce noticeable line shifts at quadrature when our observations were made. Using numerical experiments, we estimate that the difference in observed line velocity between the two quadratures should be $\sim$11 km s^{-1} if the G5 star accounts for 5% of the line flux, $\sim$7 km s^{-1} if it accounts for 3% of the line flux, and $\sim$2 km s^{-1} if it accounts for just 1%. Most of the lines observed at $\phi = 0.24$ (Si III λ1207, O V] λ1218, and N V λ1239) are slightly blueshifted, whereas almost all of the lines observed near the opposite quadrature ($\phi = 0.64$–0.67) are redshifted relative to the K1 star, which suggests that the G5 star's flux contribution is indeed a factor that must be considered. The relatively large blueshift of the Si III λ1207 line and the relatively large redshifts of the Si II λ1533 and Al II λ1671 lines suggest that the G5 star may be a larger flux contributor to these lines than it is to the C IV, Si IV, He II, and N V lines.

Because the G5 star appears to be at least partially responsible for the observed line shifts, the redshifts seen for the lines observed at $\phi = 0.64$–0.67 are actually just upper limits for the intrinsic redshifts of the K1 star's emission lines. The K1 star's transition region lines may have small redshifts of $\sim$5 km s^{-1}, but they certainly do not have redshifts as large as those observed on the G1 star of Capella (10–25 km s^{-1}; Linsky et al. 1995b).

For Procyon, the position and width of the He II λ1640 feature were used to determine whether the line is a collisionally excited line formed at transition-region temperatures or a recombination line formed at chromospheric temperatures. The situation is more complicated for HR 1099 because of the uncertainty in the centroid of the K1 star's emission lines, due to the unknown contribution of the G5 star, and because some of HR 1099's chromospheric lines are just as broad as the transition-region lines. The line profiles of the He II, C IV, and the Mg II *h* and *k* lines are very similar for reasons that we do not fully understand (see § 4.5). However, the width of the He II line is closer to that of Mg II than it is to the broader C IV lines, suggesting that He II is a chromospheric line such as Mg II. Therefore, we have used the centroid wavelength predicted for the He II multiplet by the radiative recombination model as the rest wavelength of the He II line. The average of the two *Einstein* IPC X-ray fluxes listed for HR 1099 by Majer et al. (1986) is $f_{\rm IPC} = 1.2 \times 10^{-10}$ ergs cm^{-2} s^{-1}, which means $f_{\rm IPC}/f_{\rm He\ II} = 59$. This is larger than the ratio predicted for the radiative recombination model by Hartmann et al. (1982) by about a factor of 2. Thus, the corona of HR 1099 easily produces enough energetic radiation to account for the observed He II emission, which further supports the radiative recombination model.

The line velocity of the C III] λ1909 line is -26 km s^{-1}, according to the single-Gaussian fit (see Table 3). It seems unlikely that C III] would have a velocity so discrepant from the velocities of HR 1099's other lines. The velocities of the other three lines identified in the spectral region of C III] (the

Si III] λ1892 line and the two S I lines) are very reasonable, so an inaccurate wavelength calibration cannot be responsible. At the orbital phase of the observation ($\phi = 0.64$) any emission from the G5 star would create an apparent redshift rather than a blueshift, so the G5 star cannot be responsible for the discrepant velocity either. The feature at 1908 Å appears to be somewhat asymmetric, which may imply a blend of some sort. Therefore, we fit the feature with two Gaussians—one representing C III] emission forced to be centeed on the rest frame of the K1 star (as the Si III] line appears to be) and the other representing the emission blended with C III]. The results of the fit are illustrated in Figure 9*d* and Table 3.

We are not certain what emission line the smaller Gaussian in Figure 9*d* represents. It could be an unidentified blend, or it could represent blueshifted C III] emission produced by some transient event on the K1 star. Although the line formation temperature of C III] is somewhat higher than that of Si III], it is still difficult to understand why such an event would not have also produced Si III] emission. The observation of the 1880–1920 Å spectral region consisted of two readouts of roughly 4 minutes each. There are no large, obvious profile differences between the two readouts that would indicate that flares or other transient processes are at work here, but the individual readouts are very noisy, so it is difficult to say for sure.

4.3. *Electron Density of the Transition Region*

Our attempt to derive a transition-region density for Procyon in § 3.3 using the O IV] lines was not very successful because of the weakness of the lines and the presence of blends. The situation is better for HR 1099 because there are no obvious blends. In particular, there is no sign of the S IV] λ1406.1 line, which means we do not have to worry about the S IV] λ1404.8 line contaminating the O IV] line at that wavelength. The weak O IV] lines are noisy, though, so the 1384–1420 Å spectral region in Figure 2 has been smoothed somewhat to reveal these lines. We fitted all four O IV] lines simultaneously (and also the Si IV λ1403 line that is slightly blended with the O IV] lines) and forced the O IV] lines to have the same width and velocity to further constrain the fit (see Table 3). The fluxes of the weaker O IV] lines of HR 1099 have been measured accurately enough to obtain a good density estimate, which was not the case for Procyon. We find that the fluxes of the λ1399.8 and λ1407.4 lines are essentially the same, which is consistent with the atomic model (Cook et al. 1995).

Three density-dependent flux ratios can be constructed: $R_1 = f_{1407}/f_{1401} = 0.204 \pm 0.025$, $R_2 = f_{1407}/f_{1405} = 0.57 \pm 0.10$, and $R_3 = f_{1405}/f_{1401} = 0.355 \pm 0.060$. Since the fluxes of the λ1407.4 and λ1399.8 lines are the same, as they should be for all densities, we use the average of the fluxes of the two lines for f_{1407}. The electron densities implied by these three ratios are $\log n_e = 10.04^{+0.28}_{-0.57}$ for R_1, $\log n_e = 9.83^{+0.19}_{-0.20}$ for R_2, and $\log n_e = 9.74^{+0.29}_{-0.23}$ for R_3. These three densities are reasonably consistent with each other, and they collectively imply a density of $\log n_e = 9.85 \pm 0.15$, which indicates a pressure at $\log T = 5.2$ of $\log P_e = 15.05 \pm 0.15$. This pressure is nearly identical to pressures found for Capella's transition region and the quiet solar transition region (Linsky et al. 1995b; Dere & Mason 1993). We were surprised that HR 1099, Capella, and the Sun all have similar transition-region densities and pressures, considering that the emission-line surface fluxes of HR 1099 are about 4 times as large as those of Capella and more than 100 times larger than those of the Sun. Since the very large surface fluxes of HR 1099 do not appear to be caused by higher densities and pressures, they must be due to a larger filling factor and/or a more radially extended emitting region.

Using the Si IV $\lambda\lambda$(1394+1403)/C III] λ1909 flux ratio for HR 1099, Byrne et al. (1987) derived a pressure at $\log T = 4.8$ of $\log P_e = 15.3$. The Si IV and C III] fluxes we have measured are similar to the fluxes they measured from their *IUE* data, so we would derive a similar pressure from our data. The pressure at $\log T = 4.8$ is slightly higher than the pressure at $\log T = 5.2$, which is what is expected for an atmosphere in hydrostatic equilibrium because of the weight of the overlying atmosphere (see, e.g., Brown & Jordan 1981).

4.4. *Line Widths and Opacities*

Unlike Procyon, the widths of HR 1099's emission lines cannot be neatly divided into narrow chromospheric features and broader transition-region lines. The only lines that can be considered narrow are the weak S I $\lambda\lambda$1900, 1915 lines and the C I λ1656 line, which have widths of ~ 50 km s^{-1}. These are certainly chromospheric lines, but the Al II λ1671 and Si II λ1533 lines, which are also considereed chromospheric, are as broad as many of the transition-region lines (see Table 3). It is possible that this difference in width among the chromospheric lines is due to a dramatic increase in turbulence between the lower and upper chromosphere, as the S I and C I lines are probably recombination lines formed at cooler temperatures ($\log T \sim 3.8$; Judge 1986, 1988) than the collisionally excited Al II and Si II lines ($\log T \leq 4.3$; Brown et al. 1984). If this interpretation is correct, then the atmospheric structures of both Procyon and HR 1099 show large increases in turbulence within a relatively narrow temperature range (but possibly a substantial pressure range). Procyon appears to have a factor of 2 increase in turbulence somewhere between $\log T = 4.3$ (represented by the Si II λ1533 line) and $\log T = 4.7$ (sampled by the Si III λ1207 line) whereas HR 1099 shows a factor of 3 increase in turbulence somewhere between $\log T = 3.8$ and $\log T = 4.3$.

If the Al II and Si II lines have higher opacities than the S I and C I lines, opacity broadening might explain the larger line widths rather than greater turbulence. Harper et al. (1995) demonstrated that the S I λ1900/λ1915 flux ratio is sensitive to the line opacity. Based on their Figure 5, the observed S I flux ratio for HR 1099 implies an optical depth of $\tau \sim 1$ for the stronger line. Unfortunately, we have no way of estimating the optical depths of the C I, Si II, and Al II lines at this time. Future observations of optically thin chromospheric intersystem lines such as C I] λ1994, Si II] λ2350, and Al II] λ2669 may further our understanding of the physical processes taking place in the chromosphere of HR 1099.

After the S I and C I lines, the narrowest line in HR 1099's moderate-resolution spectra is N V λ1239, which is significantly narrower than other lines formed at similar temperatures (e.g., C IV, O IV]). Before trying to explain this problem, we point out that the spectral regions shown in Figure 2 were not observed simultaneously. Because HR 1099 is a highly variable object, it is conceivable that this variability could contribute to the observed differences in line profile parameters, such as the one noted for N V. We have no evidence that this is what is happening, however, especially since the Si III λ1207 line observed at the same time as N V has a width similar to those of most of the observed transition-region lines. We will assume, therefore, that we *can* intercompare line profiles observed in different spectral regions, although we cannot completely rule out the possibility of variability within our data set.

The weighted average width of the lines listed in Table 3 (excluding the S I and C I lines) is 173 ± 19 km s^{-1}, which corresponds to a most probable nonthermal velocity of 103 ± 11 km s^{-1}. This velocity is an accurate estimate of the turbulence in the K1 star's upper chromosphere and transition region if the emission lines are not significantly opacity-broadened. With the exception of Lyα, the line profiles of HR 1099 show no obvious signs of opacity effects, as long as one assumes that the broad wings of C IV, Si IV, and He II are *not* produced by opacity effects but rather are caused by particularly turbulent regions of the stellar atmosphere, as we assumed in § 4.1. Unfortunately, the Si III λ1207 line is too noisy to detect effects of opacity broadening as subtle as those seen for Procyon's Si III line.

Unlike Procyon, the C IV λ1548/λ1551 and Si IV λ1394/λ1403 flux ratios are exactly 2.0, which is the optically and effectively thin limit. The profiles of the two C IV lines and the two Si IV lines are identical, which also suggests that the lines are optically thin. This does not prove that $\tau_o < 1$ for the C IV and Si IV lines since macroturbulence can mask the effects of opacity on the line profiles, but there are certainly no obvious opacity effects present in the profiles of any HR 1099's transition-region lines. Furthermore, the optically thin intersystem lines (O V], O IV], O III], Si III], and C III]) are just as broad as the Si III, N V, Si IV, and C IV resonance lines, which demonstrates that enough turbulence is present in the atmosphere of the K1 star to account for the broad widths of the transition-region lines without any opacity broadening.

Linsky et al. (1995b) found that the widths of Capella's intersystem lines were closer to the widths of the narrow components detected in the resonance lines than to the widths of broad components. They proposed that the intersystem lines are formed predominantly in the narrow-component regions of the stellar atmosphere, implying that the density of the broad-component regions may be high enough to reduce the intersystem line flux substantially relative to the resonance-line flux. However, for various reasons, they were unable to demonstrate conclusively that the intersystem lines do not indeed have broad components. For HR 1099, we are also unable to determine conclusively whether the intersystem lines have broad components. Some evidence for extended wing emission is present in the smoothed Si III] profile in Figure 10*d*, but this is the only smoothed intersystem line profile that appears similar to the resonance line profiles. Unlike Capella, the widths of HR 1099's intersystem lines are closer to the widths of the broad components than to the widths of the narrow components. The O III], O IV], and C III] lines are in fact the broadest lines in our spectra, based on the single-Gaussian fits. This suggests that the less turbulent regions of the stellar atmosphere may have pressures high enough to inhibit intersystem line emission and that the pressure of log $P_e = 15.05$ measured using the O IV] line ratios applies only to the broad-component regions. In particular, we note that the large discrepancy between the widths of the N V and O IV] lines alluded to above suggests that these lines are not originating entirely from the same regions, despite the fact that the temperatures at which the lines are formed are nearly identical.

4.5. *The* Mg II *h and k Lines*

The Mg II *h* and *k* line profiles of HR 1099 are displayed in Figures 3 and 11. In Figure 11, we have removed the interstellar absorption features by using polynomial fits to estimate the intrinsic stellar emission in the spectral regions obscured by the absorption. The Mg II lines are the only lines we have observed in which emission from the G5 star is apparent. We performed multi-Gaussian fits to these lines to estimate the contributions of the K1 and G5 stars. We found that the K1 star's Mg II profiles could be accurately represented as the sum of two Gaussians. A third Gaussian was used to represent the G5 star's emission. The results of the fits are shown in Figure 11 and Table 4. Also listed in Table 4 are the line profile parameters of the Mg II subordinate line at 2798 Å.

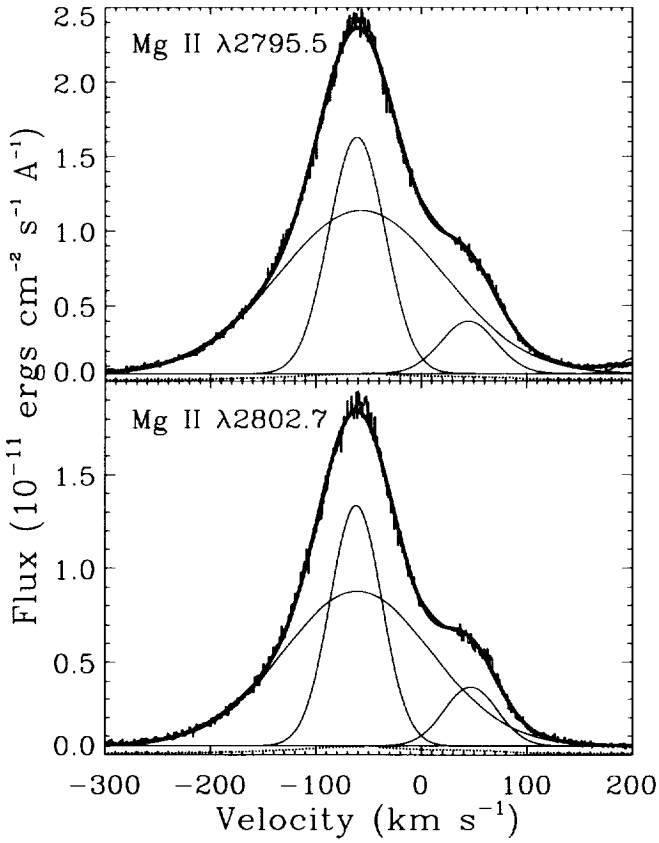

FIG. 11.—The Mg *h* (*bottom*) and *k* (*top*) line profiles of HR 1099 plotted on a heliocentric velocity scale. The 1 σ errors in the data are shown as dots. Interstellar absorption at roughly +20 km s^{-1} has been removed from both lines by use of a polynomial fit to estimate the intrinsic stellar emission above the interstellar absorption. Three-Gaussian fits were performed for both lines. The two components near −60 km s^{-1} model the emission from the K1 star, and the single component near +45 km s^{-1} represents the emission from the G5 star. The convolution of the sum of the Gaussians with the instrumental and rotational broadening profiles is shown as a thick line. The parameters for these fits are listed in Table 4.

The G5 star accounts for only ~7.5% of the Mg II line flux, according to the multi-Gaussian fits. However, since the radius of the K1 star is 3 times that of the G5 star ($R_{K1} = 3.9\ R_\odot$ and $R_{G5} = 1.3\ R_\odot$; Fekel 1983), the Mg II surface fluxes of the K1 star are only ~37% higher than those of the G5 star. Ayres et al. (1995) found a power-law slope of 1.77 ± 0.12 when stellar C IV surface fluxes were plotted versus Mg II surface fluxes. If such a relation applies to the two HR 1099 stars, then the G5 star should account for ~6% of HR 1099's C IV flux, based on its 7.5% contribution to the Mg II lines. This 6% contribution may just barely be consistent with the nondetection of the G5

TABLE 4

Mg II Line Profile Parameters for HR 1099

λ_{rest} (Å)	Component	λ_{meas} (Å)	v^a (km s^{-1})	f (10^{-12})	FWHM (km s^{-1})	χ^2_ν
2795.528.....	K1 (narrow)	2794.959	3 ± 1	9.8 ± 0.2	62 ± 1	1.494
	K1 (broad)	2794.995	7 ± 1	20.0 ± 0.3	184 ± 1	1.494
	G5	2795.945	−1 ± 1	2.2 ± 0.1	62 ± 2	1.494
2802.705.....	K1 (narrow)	2802.129	2 ± 1	7.4 ± 0.3	58 ± 2	1.300
	K1 (broad)	2802.140	4 ± 1	13.8 ± 0.3	167 ± 1	1.300
	G5	2803.144	1 ± 1	1.9 ± 0.1	59 ± 2	1.300
2797.998.....	K1	2797.414	1 ± 1	0.35 ± 0.01	34 ± 3	1.395
	G5	2798.426	0 ± 3	0.026 ± 0.006	26 ± 5	1.296

[a] Line velocity relative to the star responsible for the emission.

star's C IV emission, but we believe this value is probably a bit large (see § 4.1).

The multi-Gaussian fits suggest that the K1 star's Mg II *h* and *k* lines are slightly redshifted, with the *k* line showing the larger shift. Similar Mg II redshifts have been observed for many other late-type stars (Robinson & Carpenter 1995). The fits to HR 1099's lines also suggest that the broad component is more redshifted than the narrow component. It is difficult to be certain that these properties of the fits are real, however, because of the unquantifiable uncertainties introduced into the fits by the assumption that the G5 star's emission is exactly Gaussian and the K1 star's emission is exactly the sum of two Gaussians. The multi-Gaussian fits suggest no Doppler shifts for the G5 star's Mg II lines.

The two-Gaussian fits to the K1 star's Mg II lines look strikingly similar to the fits to the K1 star's C IV lines (see Fig. 9*b*). This similarity is shown explicitly in Figure 12. Although we found it necessary to broaden the Mg II profile by 30% to match the width of the C IV line, the agreement between the C IV and Mg II profiles in Figure 12 is still remarkable and completely unexpected. The differences that exist between the profiles are mostly due to the different Doppler shifts present in the cores and wings of the lines—the overall profile shapes are nearly identical. As discussed in § 3.5, the Mg II *h* and *k* lines are very optically thick lines whose profiles are generally interpreted in terms of opacity effects and atmospheric structure whereas the C IV line profiles are thought to be optically thin and regulated by turbulent processes. Therefore, the profiles of the Mg II and C IV lines should in general be different, but that does not appear to be the case for HR 1099.

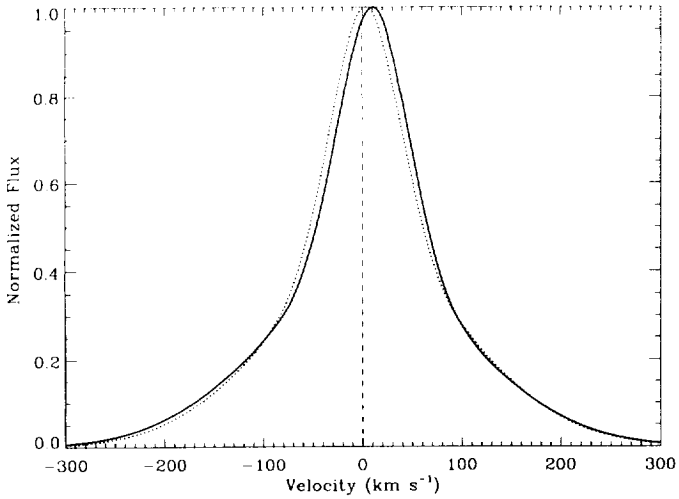

FIG. 12.—The C IV (*solid line*) and Mg II *k* (*dotted line*) line profiles of the K1 star of HR 1099, based on the two-Gaussian fits to these lines. The Mg II line has been broadened by 30% to allow a better comparison of the C IV and Mg II line profiles. If it were not for different Doppler shifts in the cores and wings of the lines, the two profiles would be essentially identical. The similarity between these two profiles is unexpected since the Mg II profile is not generally supposed to be regulated by the same turbulent processes that presumably regulate the C IV profile.

Is the similarity between the Mg II and C IV lines just a coincidence, or does it imply that the same physical processes are controlling the profiles of both lines? If not a coincidence, are the C IV lines behaving like optically thick chromospheric lines or are the Mg II lines behaving like transition-region lines? The former case would suggest that the broad wings observed for both C IV and Mg II are produced by opacity effects, whereas the latter case would suggest that the broad wings are due to particularly turbulent regions of the stellar atmosphere. It is important to determine which of these cases is correct, because if the broad wings are not caused by turbulence, then our attempts to explain the broad wings in terms of microflaring and to quantify this microflaring by using two-Gaussian fits are misguided.

We have computed theoretical Mg II profiles based on a simple, homogeneous, hydrostatic, plane-parallel model atmosphere of the K1 star to see if radiative transfer calculations predict broad line wings similar to those we have observed. Following Simon & Linsky (1980), we have based our atmospheric model on the model for ϵ Eri (K2 V) computed by Simon, Kelch, & Linsky (1980). Since the surface gravity of HR 1099's K1 star (log g = 3.40; Fekel 1983) is roughly 12.6 times lower than that of ϵ Eri, the mass column densities given for the ϵ Eri model were increased by a factor of 12.6 to maintain the same total pressure as the ϵ Eri model. This scaling increases the computed surface fluxes, which is desirable since HR 1099 has higher surface fluxes than ϵ Eri. Our model, which is displayed in Figure 13, is similar to Simon & Linsky's (1980) model A, and should be accurate enough for our very schematic calculations. A full discussion of the validity of using a scaled ϵ Eri model for HR 1099 is given by Simon & Linsky (1980).

Initially, we assumed solar abundances (see, e.g., Morton 1991) and a microturbulence model like that of Simon et al. (1980), in which the microturbulence rises from 1 km s^{-1} in the photosphere to 10 km s^{-1} for $T \geq 8000$ K. We used the radiative transfer code MULTI (Carlsson 1986) to solve for the

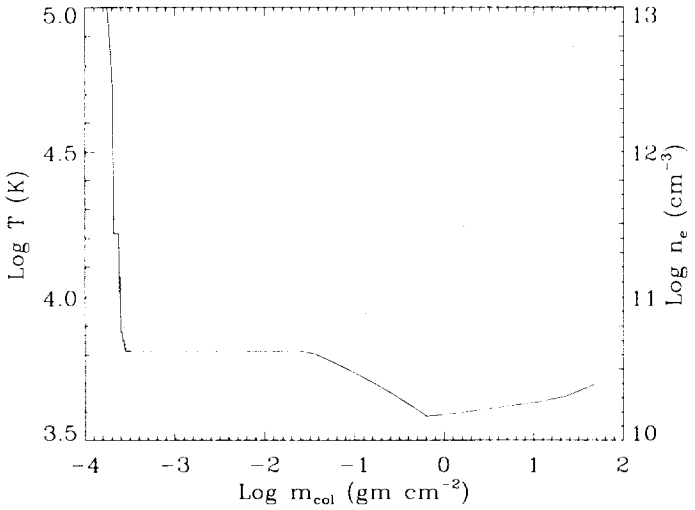

FIG. 13.—Model atmosphere for HR 1099's K1 star based on the ϵ Eri model computed by Simon et al. (1980), and very similar to Simon & Linsky's (1980) model A. The temperature (*solid line, left axis*) and electron density (*dotted line, right axis*) are plotted as functions of mass column density.

level populations of the H and Mg atomic models. For these schematic calculations we assumed complete redistribution (CRD) for hydrogen, although the method described by Carlsson & Judge (1993) was used to mimic the effects of partial redistribution (PRD) on the hydrogen ionization. For the background opacities we included non-LTE bound-free hydrogen, and all other sources were treated in LTE. For the radiative transfer calculations of the Mg II line profiles we adopted the PRD techniques of Uitenbroek (1989a, b). The Mg II model used is that given by Harper (1992). The differences between the computed Mg II resonance-line fluxes and those of Simon & Linsky (1980) are mostly due to the different treatment for hydrogen ionization.

We computed line profiles for five different values of $\mu = \cos\theta$, where θ is the angle between the normal vector of the plane-parallel atmosphere and the observer's line of sight. Three of the computed Mg II *k*-line profiles are shown in Figure 14*a*. Based on the profiles computed for the five values of μ, a disk-integrated profile is computed that allows for rotational broadening, assuming $v \sin i = 38$ km s^{-1} (Vogt & Penrod 1983). After conversion from intensity to surface-flux units, the final disk-integrated Mg II *k*-line profile is compared with the observed profile in Figure 14*b*.

The integrated surface flux of the model *k*-line profile in Figure 14*b* agrees well with the observations, and the model profile does have broad wings somewhat similar to those of the observed profile. However, the wings of the model profile are not broad enough. Also, the top of the model profile is too broad because the peaks of the self-reversed profiles in Figure 14*a* are too far apart. Further computations, which retain the original electron density stratification, have revealed that lowering the microturbulence decreases the separation between the peaks of the disk-resolved self-reversed Mg II profiles. In Figure 15 we show the disk-integrated Mg II *h* and *k* profiles that result when the microturbulence in the chromosphere is lowered from 10 to 3 km s^{-1}. The model fluxes in Figure 14 are a little too low, and this discrepancy becomes worse when the microturbulence is lowered, so we increased the magnesium abundance to 50% above solar in order to

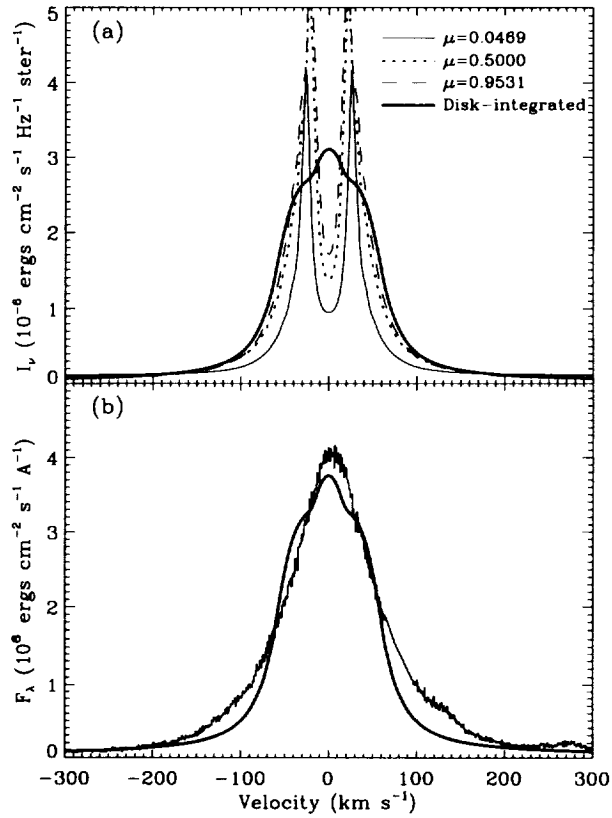

FIG. 14.—(*a*) Mg II *k*-line profiles of HR 1099's K1 star computed from the model in Fig. 13 by use of the radiative transfer code MULTI (Carlsson 1986), assuming a solar abundance for magnesium and a microturbulence of 10 km s^{-1} above $T = 8000$ K. Profiles are shown for three values of $\mu = \cos\theta$, where θ is the angle between the normal vector of the plane-parallel model atmosphere and the line of sight. A disk-integrated profile is also shown (*thick line*), with corrections for rotational broadening. (*b*) Disk-integrated profile from (*a*) compared with the observed profile. The interstellar absorption feature and the flux contribution of the G5 star (as determined by the multi-Gaussian fit in Fig. 12) have been removed from the observed profile in (*b*). The velocity scale is in the rest frame of the K1 star.

produce model profiles in Figure 15 with fluxes that better match the observations. As in Figure 14*b*, the bases of the theoretical profiles in Figure 15 are too narrow, so we have broadened the lines further by adding a macroturbulence of 40 km s^{-1}. The resulting profiles (*dotted lines*) match the observations better.

Besides the *h* and *k* lines, we have also modeled the much weaker Mg II subordinate line at 2798 Å (centered at 270 km s^{-1} in the top panel of Fig. 15). Our models do not show the subordinate line in emission when the opacities described above are used. Since this line is located in the wing of the Mg II *k* line and we have not modeled the line overlap, we arbitrarily increased the contribution from the LTE opacities by a factor of 2 to mimic the increased opacity due to the *k* line, and the subordinate line then appeared in emission as shown in the top panel of Figure 15. Previous studies of this feature (e.g., Lemaire & Gouttebroze 1983) have shown that the formation of this line is expected to be sensitive to blending with the Mg II resonance lines. This line has been observed in emission above the solar limb (Feldman & Doschek 1977) and also in the spectrum of γ Cru (M3.4 III), where fluorescence by Lyβ may be important (Carpenter, Robinson, & Judge 1995).

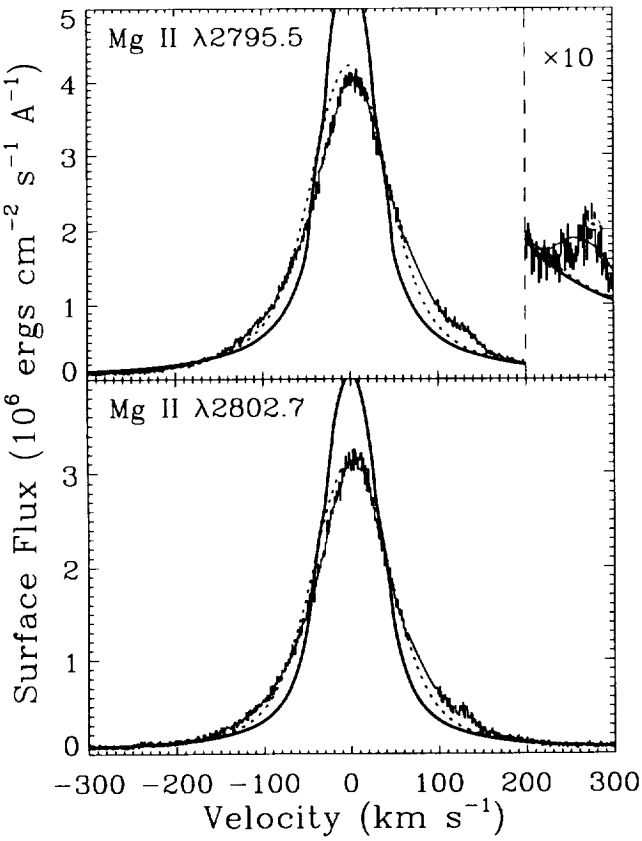

FIG. 15.—Disk-integrated Mg II *h* (*bottom*) and *k* (*top*) line profiles computed as in Fig. 14, but with a microturbulence of 3 km s^{-1} and with a magnesium abundance 50% higher than solar. The initial model profiles are shown as thick solid lines and are compared with the observed profiles that are plotted in histogram form. Interstellar absorption and the G5 star's emission (as determined by the multi-Gaussian fits in Fig. 12) have been removed from the observed profiles. A better match between the computed and observed profiles can be obtained by adding a macroturbulence of 40 km s^{-1} to the model profiles, which leads to the profiles shown as dotted lines. We have also modeled the Mg II subordinate line at 2798 Å (centered at 270 km s^{-1} in the top panel), and the computed profile for this line is shown as a thin solid line. The fluxes between 200 and 300 km s^{-1} have been increased by a factor of 10 to better display the weak subordinate line. The velocity scale is in the rest frame of the K1 star.

Since our model Mg II *h* and *k* line profiles have broad wings and fit the observed profiles fairly well when some macroturbulence is added, it seems natural to propose that opacity and radiative transfer effects are the most important factors regulating the profiles of these lines. However, despite the similarity between the Mg II and C IV line profiles, it is very difficult to believe that similar processes could be controlling the C IV profiles. Solar C IV lines are limb-brightened (Kjeldseth-Moe & Nicolas 1977), implying optical depths much too low for opacity effects to induce broad emission wings.

The optical depth of HR 1099's C IV lines can be estimated by use of equation (5). In computing the observed surface flux F, we assume a stellar radius of 3.9 $R_\odot$ (Fekel 1983), and we assume that the C IV emission is uniform over the stellar surface. For $\Omega = 6.4$ (Cochrane & McWhirter 1983), $g = 2$, $f = 0.1908$ (Morton 1991), and log $P_e = 15.05$ (see § 4.3), we find that $\tau_o = 0.72/\Delta\lambda$ for the stronger C IV line.

It is important to be aware that $\Delta\lambda$ in this equation is the line width associated only with the microturbulence. Only if opacity broadening and macroturbulence are unimportant can the observed width listed in Table 3 (FWHM = 194 km s^{-1} = 1.0 Å) be used for $\Delta\lambda$. Otherwise, the observed width is only an upper limit for $\Delta\lambda$. A lower limit to the microturbulence present in the C IV line is that due to thermal motions, $\Delta\lambda = 0.10$ Å. Using this lower limit, we calculate an upper limit for the optical depth of the C IV λ1548 line of $\tau_o < 7.2$. The only way that τ_o can be significantly larger than 7.2 is if the C IV emission in reality originates from a very small area on the stellar surface, meaning we have grossly underestimated the true C IV surface flux. We believe that τ_o must be at least 1000 for opacity effects to produce broad wings, so it is highly improbable that the line wings of C IV are produced by radiative transfer effects. Considering also the very broad widths of the optically thin transition-region intersystem lines, the evidence for turbulence-dominated C IV profiles is overwhelming. For comparison, we note that equation (5) predicts $\tau_o \sim 10{,}000$ for the Mg II *k* line, which illustrates why our Mg II model profiles have opacity-broadened emission wings.

Despite some success in reproducing the observed profiles of the Mg II lines with radiative transfer models, we find it very unlikely that the C IV lines are also regulated by radiative transfer effects. Therefore, either the similarity between the Mg II and C IV profiles is simply coincidental or the moderate success of the Mg II models is misleading and turbulence actually plays a much larger role in shaping the line profiles than the models suggest. To investigate this latter possibility further, we modeled the Si II λ1533 line, assuming a solar silicon abundance, PRD, the Si II model used by Harper (1992), and a microturbulence of 3 km s^{-1} (as in the Mg II model in Fig. 15). The result is shown in Figure 16. Our calculated surface flux for this line is too high by about a factor of 2, so we have divided the calculated fluxes by 2 in Figure 16 to allow for

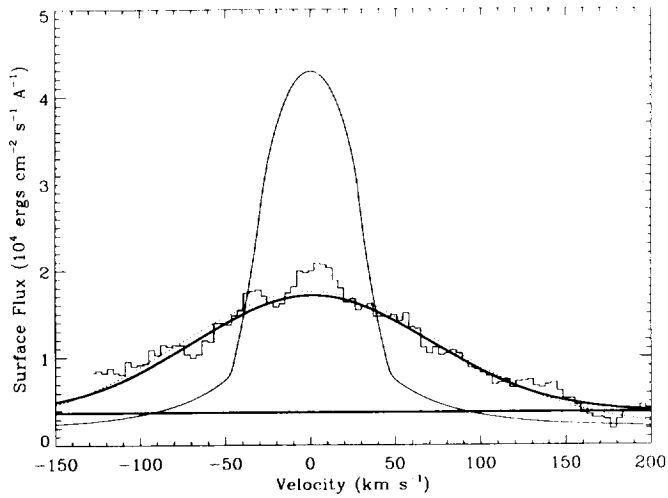

FIG. 16.—Observed Si II λ1533 line profile (*histogram*) and the single-Gaussian fit to the line and flat continuum assumed for the fit (*thick solid lines*). The velocity scale is centered on the centroid of the observed profile, which is redshifted relative to the K1 star by 13 km s^{-1} (see Table 3). The thin solid line is a Si II profile computed based on the atmospheric model in Fig. 13, assuming a solar silicon abundance and a microturbulence of 3 km s^{-1}. The computed fluxes of this model were actually twice as high as those shown in the figure. We have divided the fluxes by 2 to allow for easier comparison of the computed and observed profiles. Adding a macroturbulence of 100 km s^{-1} to the model profile leads to the profile shown as a dotted line, which fits the data better.

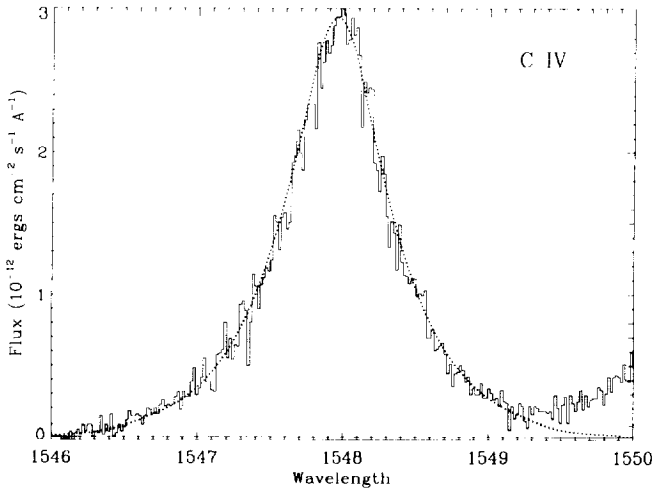

FIG. 17.—Alternative line profile model to the two-component model in Fig. 9*b*. If the line profiles being produced by different regions of HR 1099's atmosphere are Gaussian and have a normal distribution of widths (with a mean of 205 km s^{-1} and σ = 100 km s^{-1}), the dotted line is the resulting disk-averaged line profile, which matches the observed profile (*histogram*) quite well.

easier comparison between the modeled and observed Si II profiles. The model Si II line is found to have broad emission wings, but they are not as prominent or as broad as those of Mg II. However, the *observed* Si II line profile is actually somewhat broader than the observed Mg II lines, and the width of the model Si II profile is therefore much too narrow. The observed line width can be reproduced only if a macroturbulence of 100 km s^{-1} is added to the model profile, as shown in Figure 16. In such a model, macroturbulence actually plays a larger role in shaping the line profile than do the radiative transfer effects, suggesting that the K1 star's chromosphere may in fact contain significant turbulence. Therefore, it at least seems possible that the broad wings of the Mg II lines are in fact produced in part by turbulence. If the microflaring interpretation of the broad transition-region line wings is correct, then microflaring may also be occurring in the K1 star's chromosphere. We note that broad wings were *not* found in the chromospheric lines of Capella (Linsky et al. 1995b), so observations of other extremely active stars should be performed to determine how common broad chromospheric line wings are for active stars.

4.6. *Discussion*

Even if one accepts our assumption that the profiles of HR 1099's emission lines are regulated by turbulence, it remains open to debate whether microflaring is responsible for the particularly broad line wings and whether the broad components of the two-Gaussian fits to these lines successfully quantify the microflaring contribution. It should come as no surprise that two-Gaussian fits, which imply two distinct emission components with different degrees of turbulence, are not unique models of these profiles. The flaring solar transition-region line profiles discussed by Cheng (1990) are very similar to the C IV profiles of HR 1099, which suggests that *all* of HR 1099's transition-region line emission may be generated by microflaring.

Figure 17 demonstrates that one can interpret HR 1099's C IV profiles in terms of a single, normal distribution of line widths being emitted from the stellar surface. Assuming such a distribution may be reasonable because solar observations show that the widths of the C IV lines are not the same everywhere on the solar disk (Dere & Mason 1993). Neither do all solar flares and transition-region explosive events produce identical line profiles (e.g., Cheng 1990; Dere et al. 1989).

However, the solar example also suggests that a two-component model may be meaningful because the line profiles of transition-region explosive events are produced by a phenomenon separate and distinct from the less dynamic processes that generate the narrower emission lines that are much more prevalent on the Sun. Therefore, it is not correct to claim that the widths of the very broad lines produced by the explosive events simply represent the high-velocity tail of a single solar transition-region line width distribution. It is more accurate to say that there are two separate distributions—one with relatively narrow line widths and one with broad widths. On the Sun, the narrow distribution completely dominates the disk-averaged line profile, but since the explosive events certainly appear to be a manifestation of stellar activity, this does not have to be the case on stars as active as HR 1099. It is natural to suppose that the explosive-event phenomenon may be a lot more prevalent on active stars, which nicely explains the broad line wings that have been observed in some of these stars, including HR 1099, and it explains why the lines of Procyon, a less active star, do not have the broad wings. However, we cannot rule out the possibility that differences in spectral type may produce effects that could also be at least partially responsible for the differences in the line profiles of HR 1099 and Procyon.

Besides the broad transition-region line wings, other observed properties of active stars are also suggestive of continuous microflaring. On the Sun, coronal temperatures above 10^7 K are observed only during solar flares, but very active stars such as HR 1099 have coronal temperatures this high even when they are not obviously flaring (see, e.g., Dempsey et al. 1993). The implication is that continuous small-scale flaring may be maintaining the very high coronal temperatures (Haisch, Strong, & Rodonò 1991). Observations of active stars and solar flares have demonstrated that their X-ray luminosities are strongly correlated with their microwave luminosities. Because the same linear relation appears to apply to both the solar flares and the "quiescent" emission from the active stars, these studies suggest that the microwave and X-ray emission observed from active stars is produced by flare-like processes (Güdel 1994; Benz & Güdel 1994).

All of this evidence suggests that microflaring is very prevalent in the atmospheres of active stars. If the broad UV emission-line wings observed for HR 1099 and other active stars are in fact spectral signatures of this microflaring, then these UV line profiles give us a unique opportunity to study the properties of the microflares. Understanding this microflaring is very important, as many authors have proposed that microflaring may be the dominant source of coronal heating for the Sun and other stars (see, e.g., Porter et al. 1987; Parker 1988; references therein).

5. SUMMARY

In this paper we have analyzed high-quality GHRS observations of both Procyon and HR 1099 in order to compare the atmospheric properties of a relatively inactive star with those of an extremely active star. The results of our analysis of the Procyon data are summarized as follows:

1. With the exception of the N v λ1239 line, Procyon's transition-region lines do not have the broad wings that have been observed on active stars, supporting our contention that the broad wings are probably a manifestation of stellar activity and may be caused by microflaring. Observations of other inactive stars are needed to determine conclusively whether inactive stars as a group do not have broad components in their transition-region lines.

2. Procyon's transition-region lines have redshifts very similar to the redshifts observed on the Sun. We find the redshifts increase gradually with temperature, rising from +4 km s^{-1} at log $T = 4.7$ to +11 km s^{-1} at log $T = 5.4$. Line redshifts such as these may indicate the presence of a circulation system in which most of the transition-region line flux is produced by the downward leg of the system.

3. Procyon's strong transition-region lines all have blue-wing excesses. The cause of these excesses is uncertain, but perhaps they are spectral signatures of the upward leg of the aforementioned circulation system.

4. The He II λ1640 line is probably formed in Procyon's chromosphere since the line's velocity and width are similar to those of other chromospheric lines but are not consistent with the transition-region lines. This suggests that the radiative recombination line formation model, rather than the collisional excitation model, is appropriate for Procyon.

5. The O IV] density diagnostics indicate transition-region pressures of log $P_e < 15.5$. This upper limit is inconsistent with the coronal pressures measured from *EUVE* data (log $P_e = 16.0$). The simplest explanation for this discrepancy is that Procyon's atmosphere must be inhomogeneous.

6. The emission lines of Procyon are significantly broader than those of the Sun. Except for O IV], Procyon's transition-region lines all have essentially the same width, FWHM = 78.7 ± 0.9 km s^{-1}, which implies nonthermal velocities of $\xi = 46.1 \pm 0.5$ km s^{-1} in the transition region. Procyon's narrower chromospheric lines also have essentially the same width, FWHM = 39.6 ± 2.3 km s^{-1}, which implies $\xi = 22.7 \pm 1.6$ km s^{-1} in the chromosphere.

7. The Si III λ1207 line is the only transition-region line profile we have observed that is obviously altered by opacity effects. Our crude analysis of the Si III profile suggests that $\tau_o = 0.7$ for the line, but we consider this to be only a lower limit to the actual optical depth. Based on this lower limit, we derive an upper limit for the electron pressure of log $P_e < 14.8$. We note that this calculation relies on a stellar line surface flux computed under the assumption that the Si III emission is uniformly distributed over the stellar surface.

8. The Mg II *h* and *k* line profiles of Procyon are very similar to those of the Sun. The line profiles are self-reversed and have stronger blue peaks, which are probably signatures of hydrodynamical processes in the chromosphere.

The results of our analysis of the GHRS observations of HR 1099 are summarized as follows:

1. The K1 star accounts for nearly all of HR 1099's UV line emission. Emission from the G5 star was detected only in the Mg II *h* and *k* lines, where it is responsible for ~7.5% of HR 1099's Mg II flux. It must be responsible for only ~5% or less of HR 1099's C IV, Si IV, and He II flux to explain the nondetection of the G5 star's emission in those lines.

2. Broad non-Gaussian wings were detected in four of HR 1099's strongest UV emission lines: Si IV λ1394, C IV $\lambda\lambda$1548, 1551, and He II λ1640. The broad components of the two-Gaussian fits to these lines account for 65.6% $\pm$ 1.0% of the total line flux. For comparison, the broad components of AU Mic and Capella account for ~40% of the line flux. Since HR 1099 is more active than both AU Mic and Capella, the larger broad-component contribution for HR 1099 is consistent with a correlation between the broad components and stellar activity and is consistent with the hypothesis that microflaring is responsible for the broad-component emission. After smoothing the data, we find that the N v λ1239, Al II λ1671, and Si III] λ1892 lines may also have profiles similar to those of Si IV, C IV, and He II.

3. The broad components of the C IV and He II lines are blueshifted relative to the narrow components. Linsky et al. (1995b) discovered that many of the transition-region lines of Capella have the same property.

4. The transition-region lines of the K1 star of HR 1099 probably have intrinsic redshifts no larger than +5 km s^{-1}, in contrast to the large 10–25 km s^{-1} redshifts observed on the active G1 III star of Capella.

5. The profiles of the K1 star's C IV $\lambda\lambda$1548, 1551, Mg II *h* and *k*, and He II λ1640 lines are very similar. Since the width of the He II line is closer to that of the Mg II lines than to the broader C IV lines, we have proposed that the He II line is formed in the chromosphere by radiative recombination. The extremely large X-ray surface flux of the K1 star supports this conclusion.

6. Using the density-sensitive O IV] lines, we derived a transition-region pressure (in units of cm^{-3} K) of log $P_e = 15.05 \pm 0.15$. This pressure is similar to transition-region pressures measured for Capella and the quiet Sun. This is surprising, considering that the transition-region line surface fluxes of HR 1099 are about 4 times larger than those of Capella and more than 100 times larger than those of the Sun.

7. The S I and C I lines are much narrower (FWHM $\approx$ 50 km s^{-1}) than the widths of lines formed in the upper chromosphere and transition region (FWHM = 173 ± 19 km s^{-1}), which suggests a large increase in turbulence from the lower to the upper chromosphere.

8. We see no obvious evidence of opacity in any of the line profiles of HR 1099. The extremely broad widths of the optically thin intersystem lines suggest that nonthermal velocities control the transition-region line profiles.

9. The profiles of the C IV and Mg II lines are remarkably similar, which suggests that similar processes regulate the profiles of these lines. It is possible that microflaring may be responsible for the broad wings observed in both the C IV and Mg II lines. This would imply that, on HR 1099's K1 star, microflaring may be taking place in the chromosphere as well as in the transition region. However, radiative transfer models suggest that, for Mg II, opacity effects can in principle also account for the broad wings.

We would like to thank J. Valenti for his assistance in modeling HR 1099's Mg II lines. We would also like to thank A. Brown and J. Neff for their assistance in writing the proposals requesting the observations on which this paper is based, and the anonymous referee for many useful comments. This research has made use of the SIMBAD database, operated at CDS, Strasbourg, France. This work is supported by NASA Interagency Transfer S-56460-D to the National Institute of Standards and Technology.

REFERENCES

Achour, H., Brekke, P., Kjeldseth-Moe, O., & Maltby, P. 1995, ApJ, 453, 945
Athay, R. G. 1988, Sol. Phys., 116, 223
Ayres, T. R. 1991, ApJ, 375, 704
Ayres, T. R., et al. 1995, ApJS, 96, 223
Ayres, T. R., Jensen, E., & Engvold, O. 1988, ApJS, 66, 51
Ayres, T. R., & Linsky, J. L. 1982, ApJ, 254, 168
Ayres, T. R., Linsky, J. L., & Shine, R. A. 1974, ApJ, 192, 93
Ayres, T. R., Marstad, N. C., & Linsky, J. L. 1981, ApJ, 247, 545
Ayres, T. R., Stencel, R. E., Linsky, J. L., Simon, T., Jordan, C., Brown, A., & Engvold, O. 1983, ApJ, 274, 801
Bartolini, C., et al. 1983, A&A, 117, 149
Benz, A. O., & Güdel, M. 1994, A&A, 285, 621
Bevington, P. R., & Robinson, D. K. 1992, Data Reduction and Error Analysis for the Physical Sciences (2d ed.; New York: McGraw-Hill)
Brandt, J. C., et al. 1994, PASP, 106, 890
Brekke, P. 1993, ApJ, 408, 735
Brown, A. 1994, in ASP Conf. Proc. 64, Cool Stars, Stellar Systems, and the Sun, ed. J.-P. Caillault (San Francisco: ASP), 23
Brown, A., & Jordan, C. 1981, MNRAS, 196, 757
Brown, A., Jordan, C., Stencel, R. E., Linsky, J. L., & Ayres, T. R. 1984, ApJ, 283, 731
Brueckner, G. E., & Bartoe, J.-D. F. 1983, ApJ, 272, 329
Brueckner, G. E., Bartoe, J.-D. F., Cook, J. W., Dere, K. P., Socker, D., Kurokawa, H., & McCabe, M. 1988, ApJ, 335, 986
Byrne, P. B., Doyle, J. G., Brown, A., Linsky, J. L., & Rodonò, M. 1987, A&A, 180, 172
Carlsson, M. 1986, A Computer Program for Solving Multi-Level Non-LTE Radiative Transfer Problems in Moving or Static Atmospheres (Uppsala Astron. Obs. Rep. 33) (Uppsala: Uppsala Univ.)
Carlsson, M., & Judge, P. G. 1993, ApJ, 402, 344
Carpenter, K. G., Robinson, R. D., & Judge, P. G. 1995, ApJ, 444, 424
Cheng, C.-C. 1990, ApJ, 349, 362
Cheng, Q. Q. 1992, A&A, 262, 581
Cochrane, D. M., & McWhirter, R. W. P. 1983, Phys. Scr., 28, 25
Cook, J. W., & Brueckner, G. E. 1991, in Solar Interior and Atmosphere, ed. A. N. Cox, W. C. Livingston, & M. S. Matthews (Tucson: Univ. Arizona Press), 996
Cook, J. W., Keenan, F. P., Dufton, P. L., Kingston, A. E., Pradhan, A. K., Zhang, H. L., Doyle, J. G., & Hayes, M. E. 1995, ApJ, 444, 936
Dempsey, R. C., Linsky, J. L., Schmitt, J. H. M. M., & Fleming, T. A. 1993, ApJ, 413, 333
Dempsey, R. C., Neff, J., & Linsky, J. L. 1996, in preparation
Dere, K. P., Bartoe, J.-D. F., & Brueckner, G. E. 1983, ApJ, 267, L65
———. 1989, Sol. Phys., 123, 41
Dere, K. P., Bartoe, J.-D. F., Brueckner, G. E., Cook, J. W., & Socker, D. G. 1987, Sol. Phys., 114, 22
Dere, K. P., & Mason, H. E. 1993, Sol. Phys., 144, 217
Donnelly, R. F., White, O. R., & Livingston, W. C. 1994, Sol. Phys., 152, 69
Dorren, J. D., & Guinan, E. F. 1990, ApJ, 348, 703
Doschek, G. A., Feldman, U., & Bohlin, J. D. 1976, ApJ, 205, L177
Drake, J. J., Laming, J. M., & Widing, K. G. 1995, ApJ, 443, 393
Dravins, D., & Nordlund, Å. 1990a, A&A, 228, 184
———. 1990b, A&A, 228, 203
Dufton, P. L., & Kingston, A. E. 1989, MNRAS, 241, 209
Duncan, D. K. 1992, Goddard High Resolution Spectrograph Instrument Handbook, Version 3.0 (Baltimore: STScI)
Fekel, F. C. 1983, ApJ, 268, 274
Feldman, U., & Doschek, G. A. 1977, ApJ, 212, L147
Feldman, U., Doschek, G. A., & Mariska, J. T. 1979, ApJ, 229, 369
Feldman, U., Doschek, G. A., VanHoosier, M. E., & Tousey, R. 1975, ApJ, 199, L67
Feldman, U., & Laming, J. M. 1994, ApJ, 434, 370
Gilliland, R. L., & Hulbert, S. J. 1993, Line Spread Functions for GHRS Spectra with the LSA (GHRS Instrum. Sci. Rep. 055) (Baltimore: STScI)
Gray, D. F. 1982, ApJ, 258, 201
Griffin, R. 1971, MNRAS, 155, 139
Güdel, M. 1994, ApJS, 90, 743
Haisch, B., Strong, K. T., & Rodonò, M. 1991, ARA&A, 29, 275
Harper, G. M. 1992, MNRAS, 256, 37
Harper, G. M., Wood, B. E., Linsky, J. L., Bennett, P. D., Ayres, T. R., & Brown, A. 1995, ApJ, 452, 407
Hartmann, L., Dupree, A. K., & Raymond, J. C. 1982, ApJ, 252, 214
Heap, S. R., et al. 1995, PASP, 107, 871
Irwin, A. W., Fletcher, J. M., Yang, S. L. S., Walker, G. A. H., & Goodenough, C. 1992, PASP, 104, 489
Jordan, C., Brown, A., Walter, F. M., & Linsky, J. L. 1986, MNRAS, 218, 465
Judge, P. G. 1986, MNRAS, 221, 119
———. 1988, MNRAS, 231, 419
Kjeldseth-Moe, O., & Nicolas, K. R. 1977, ApJ, 211, 579
Lemaire, P., & Gouttebroze, P. 1983, A&A, 125, 241
Lemen, J. R., Mewe, R., Schrijver, C. J., & Fludra, A. 1989, ApJ, 341, 474
Lenz, D. D., & Ayres, T. R. 1992, PASP, 104, 1104
Linsky, J. L., & Ayres, T. R. 1978, ApJ, 220, 619
Linsky, J. L., et al. 1993, ApJ, 402, 694
Linsky, J. L., Diplas, A., Wood, B. E., Brown, A., Ayres, T. R., & Savage, B. D. 1995a, ApJ, 451, 335
Linsky, J. L., & Wood, B. E. 1994, ApJ, 430, 342
Linsky, J. L., Wood, B. E., Judge, P., Brown, A., Andrulis, C., & Ayres, T. R. 1995b, ApJ, 442, 381
Majer, P., Schmitt, J. H. M. M., Golub, L., Harnden, F. R., Jr., & Rosner, R. 1986, ApJ, 300, 360
McClymont, A. N., & Craig, I. J. D. 1987, ApJ, 312, 402
Mihalas, D. M. 1978, Stellar Atmospheres (2d ed.; San Francisco: W. H. Freeman)
Morton, D. C. 1991, ApJS, 77, 119
Mullan, D. J., & Cheng, Q. Q. 1994, ApJ, 435, 435
Nordlund, Å., & Dravins, D. 1990, A&A, 228, 155
Parker, E. N. 1988, ApJ, 330, 474
Porter, J. G., Moore, R. L., Reichman, E. J., Engvold, O., & Harvey, K. L. 1987, ApJ, 323, 380
Reale, F., Peres, G., & Serio, S. 1995, A&A, in press
Robinson, R. D., Blackwell, J., Feggans, K., Lindler, D., Norman, D., & Shore, S. N. 1992, A User's Guide to the GHRS Software, Version 2.0 (Greenbelt, MD: GSFC)
Robinson, R. D., & Carpenter, K. G. 1995, ApJ, 442, 328
Rutten, R. J., & Uitenbroek, H. 1991, Sol. Phys., 134, 15
Sandlin, G. D., Bartoe, J.-D. F., Brueckner, G. E., Tousey, R., & VanHoosier, M. E. 1986, ApJS, 61, 801
Schmitt, J.-H. M. M., Collura, A., Sciortino, S., Vaiana, G. S., Harnden, F. R., Jr., & Rosner, R. 1990, ApJ, 365, 704
Schmitt, J. H. M. M., Haisch, B. M., & Drake, J. J. 1994, Science, 265, 1420
Simon, T., Kelch, W. L., & Linsky, J. L. 1980, ApJ, 237, 72
Simon, T., & Linsky, J. L. 1980, ApJ, 241, 759
Steffen, M. 1985, A&AS, 59, 403
Strand, K. A. 1951, ApJ, 113, 1
Strassmeier, K. G., Hall, D. S., Zeilik, M., Nelson, E., Eker, Z., & Fekel, F. C. 1988, A&AS, 72, 291
Uitenbroek, H. 1989a, A&A, 213, 360
———. 1989b, A&A, 216, 310
Vogt, S. S., & Penrod, G. D. 1983, PASP, 95, 565
Wahlstrom, C., & Carlsson, M. 1994, ApJ, 433, 417
Wood, B. E., Brown, A., Linsky, J. L., Kellett, B. J., Bromage, G. E., Hodgkin, S. T., & Pye, J. P. 1994, ApJS, 93, 287